Revista ALCONPAT
www.revistaalconpat.org
eISSN 2007-6835
Revista de la Asociación Latinoamericana de Control de Calidad, Patología y Recuperación de la Construcción

# Complete design for rectangular combined footings assuming that the contact area with the soil is partially compressed.

A. Luévanos Rojas[1]*, S. López Chavarría[1],
M. Medina Elizondo[1], C. Martínez Aguilar[1]
*Contact author: arnulfol_2007@hotmail.com
DOI: https://doi.org/10.21041/ra.v16i3.1021

Received: 14/02/2026 | Received in revised form: 14/04/2026 | Accepted: 10/07/2026 | Published: 01/09/2026

## ABSTRACT
This paper presents the complete design for RCFs (rectangular combined footings), assuming that the contact area with the soil is partially compressed. The formulation is carried out by integration to determine the moments, flexural shearing and punching shearing for all possible cases for footings under biaxial and uniaxial flexion. Numerical studies are presented to determine the design of this type of foundation. The proposed model offers significant savings in concrete and steel volumes compared to the current model, if the resultant force is located outside the central nucleus. Therefore, the proposed model should be used, because it offers better quality in the control of the resources used.
**Keywords:** complete design; rectangular combined footings; moments; flexural shearing; punching shearing.

**Cite as:** Luévanos Rojas, A., López Chavarría, S., Medina Elizondo, M., Martínez Aguilar, C. (2026), *"Diseño completo para zapatas combinadas rectangulares asumiendo que el área de contacto con el suelo está parcialmente comprimida"*, Revista ALCONPAT, 16 (3), pp. 422 – 474, DOI: https://doi.org/10.21041/ra.v16i3.1021

[1] Instituto de Investigaciones Multidisciplinarias, Universidad Autónoma de Coahuila, Torreón, Coahuila, México.

**Contribution of each author**
In this work, the author Arnulfo Luévanos Rojas contributed to the original idea for the article (100%), mathematical development of the new model (100%) and coordinated the work in general (100%). The author Sandra López Chavarría contributed to the discussion of results (100%). The author Manuel Medina Elizondo contributed to the writing of the work (100%). The author Carmela Martínez Aguilar contributed to the elaboration of the figures (100%) and the application of the proposed model (100%).



**Discussions and subsequent corrections to the publication**
Any dispute, including the replies of the authors, will be published in the second issue of 2026 provided that the information is received before the closing of the first issue of 2026.

# Diseño completo para zapatas combinadas rectangulares asumiendo que el área de contacto con el suelo está parcialmente comprimida.


## RESUMEN

Este trabajo presenta el diseño completo para ZCRs (zapatas combinadas rectangulares), asumiendo que la superficie de contacto con el suelo está parcialmente comprimida. La formulación se lleva a cabo por integración para determinar los momentos, los cortantes por flexión y los cortantes por punzonamiento para todos los casos posibles para zapatas bajo flexión biaxial y uniaxial. Los estudios numéricos se presentan para determinar el diseño de este tipo de zapatas. El modelo propuesto presenta un ahorro significativo en los volúmenes de acero y concreto que el modelo actual, si la fuerza resultante se localiza fuera del núcleo central. Por lo tanto, el modelo propuesto se debe de utilizar, porque presenta mejor calidad en el control de los recursos utilizados.


**Palabras clave:** diseño completo; zapatas combinadas rectangulares; momentos; cortantes por flexión; cortantes por punzonamiento.

# Dimensionamento completo de sapatas combinadas retangulares, considerando que a área de contato com o solo está parcialmente comprimida.


## RESUMO

Este trabalho apresenta o dimensionamento completo de ZCRs (sapatas combinadas retangulares), considerando que a superfície de contato com o solo está parcialmente comprimida. A formulação é desenvolvida por meio de integração para determinar os momentos, os esforços cortantes por flexão e os esforços cortantes por punção para todos os casos possíveis de sapatas submetidas à flexão biaxial e uniaxial. São apresentados estudos numéricos para determinar o dimensionamento desse tipo de sapata. O modelo proposto apresenta uma economia significativa nos volumes de aço e concreto em comparação com o modelo atual, quando a força resultante está localizada fora do núcleo central. Portanto, recomenda-se a utilização do modelo proposto, uma vez que proporciona melhor controle e otimização dos recursos empregados.


**Palavras-chave**: dimensionamento completo; sapatas combinadas retangulares; momentos; esforços cortantes por flexão; esforços cortantes por punção.

**Legal Information**

Revista ALCONPAT is a quarterly publication by the Asociación Latinoamericana de Control de Calidad, Patología y Recuperación de la Construcción, Internacional, A.C., Km. 6 antigua carretera a Progreso, Mérida, Yucatán, 97310, Tel. +52 1 983 419 8241, alconpat.int@gmail.com, Website: www.alconpat.org

Reservation of rights for exclusive use No.04-2013-011717330300-203, and ISSN 2007-6835, both granted by the Instituto Nacional de Derecho de Autor. Responsible editor: Pedro Castro Borges, Ph.D. Responsible for the last update of this issue, Informatics Unit ALCONPAT, Elizabeth Sabido Maldonado.

The views of the authors do not necessarily reflect the position of the editor.

# 1. INTRODUCTION

The dimensions of the footings also depend on the size and type of structure to be built. Proper footing placement is crucial to provide adequate support for the foundation and, ultimately, for the structure.

Shallow foundations must meet certain design requirements:

Safety against the load-bearing capacity, that is, exceeding the shear strength of the underlying soil; Control of excessive settlements that may damage the overlying structure or affect functionality.

The soil bearing capacity has been studied for shallow foundations under biaxial flexure, which considers a linear distribution of soil pressure and a partially compressed contact surface (Peck et al., 1974; Teng, 1979; Highter y Anders, 1985; Vitone y Valsangkar, 1986; Irles-Más y Irles-Más, 1992; Algin, 2000, 2001, 2007; Young y Budynas, 2002; Özmen, 2011; Rodriguez-Gutierrez y Aristizabal-Ochoa, 2004, 2013a, b; Lee et al., 2015; Kaur y Kumar, 2016; Bezmalinovic Colleoni, 2016; Dagdeviren, 2016; Aydogdu, 2016; Girgin, 2017; Al-Gahtani y Adekunle, 2019; Galvis y Smith-Pardo, 2020; Rawat et al., 2020; Lezgy-Nazargah et al., 2022; Gör, 2022).

The most important contributions to determine the minimum area and its dimensions on footings that take into account the contact surface with the soil is partially compressed: for isolated rectangular footings (Vela-Moreno et al., 2022) and circular footings (Soto-García et al., 2022; Luévanos-Soto et al., 2024a), and for ZCRs (Montes-Páramo et al., 2023), in the shape of a T (Luévanos-Rojas et al., 2025), and corner (Luévanos-Rojas, 2025a, b).

The most recent research on complete designs for footings that take into account the contact area with the soil is partially compressed are: for rectangular isolated footings (Luévanos-Rojas, 2023) and circular footings (Kim-Sánchez et al., 2022; Luévanos-Soto et al., 2024b).

Studies on the design of RCFs under uniaxial and biaxial flexure that consider a linear distribution of soil pressure have been studied by several researchers (Konapure y Vivek, 2013; Vivek et al., 2014; Luévanos-Rojas, 2014; Luévanos-Rojas, 2016a, b; Luévanos-Rojas et al., 2017, 2020; Ravi Kumar Reddy et al., 2018; Velázquez-Santillán et al., 2018). All these works take into account that the contact area with the ground is fully compressed.

According to the literature review, the closest contributions to the topic addressed in this work are: for rectangular isolated footings by Luévanos-Rojas (2023) and circular footings (Kim-Sánchez et al., 2022; Luévanos-Soto et al., 2024b). Therefore, there is no relation to the complete design theme for RCFs under uniaxial and biaxial flexure considering the contact area with the ground is partially compressed.

This document shows the complete design of RCFs to determine the thickness and areas of transverse and longitudinal steel, assuming that the contact area with the soil is partially compressed, taking into account that the sides and minimum area are known by Montes-Páramo et al. (2023). Numerical examples for biaxial flexure are shown for the four types of constraints in the Y-axis direction (unconstrained, constrained in column 1, constrained in column 2, constrained in both columns) for $L$ = 6.00 and 7.00 m. Numerical examples for uniaxial flexure are shown for two cases: 1) When the loads are located on the Y-axis (Y-case). 2) When the loads are located on the X-axis (X-case). A comparison is also made between the current model and the model proposed in this article to observe the differences. This model will be of great help to building contractors, as it offers better quality control over the resources used (labor, materials, small equipment, etc.) because it adapts to the actual soil conditions. Therefore, it leads to greater savings in these types of structural elements.

## 2. FORMULATION OF THE PROPOSED MODEL

Figure 1 shows a rigid RCF under an axial load, a moment about the X-axis, and a moment about the Y-axis at each column.

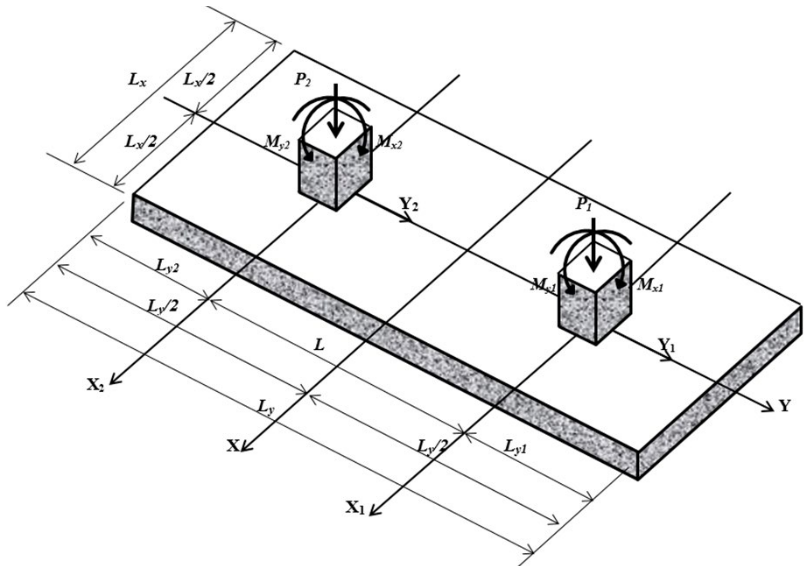


Figure 1. RCF subjected to biaxial flexure.
Source: Own elaboration

Rigid RCFs deform in a flat shape, that is, the soil pressure distribution diagram is assumed to be linear under the footing.
The general equations for bending of RCFs due to factored loads are (Montes-Páramo et al. 2023):
Biaxial flexure:
The pressure in the main direction (Y-axis) is:

$$\sigma_u(x, y) = \frac{R_u}{L_x L_y} + \frac{12 M_{uxT} y}{L_x {L_y}^3} + \frac{12 M_{uyT} x}{{L_x}^3 L_y} \tag{1}$$

The pressure in the direction transverse to the main direction (X axis), for $P_{u1}$ on the $X_1$ and $Y_1$ axes is:

$$\sigma_{uP1}(x_1, y_1) = \frac{P_{u1}}{L_x w_1} + \frac{12 M_{ux1} y_1}{L_x {w_1}^3} + \frac{12 M_{uy1} x_1}{{L_x}^3 w_1} \tag{2}$$

The pressure in the direction transverse to the main direction (Y axis), for $P_{u2}$ on the $X_2$ and $Y_2$ axes is:

$$\sigma_{uP2}(x_2, y_2) = \frac{P_{u2}}{L_x w_2} + \frac{12 M_{ux2} y_2}{L_x {w_2}^3} + \frac{12 M_{uy2} x_2}{{L_x}^3 w_2} \tag{3}$$

Uniaxial flexure ($R_u$ is located on the Y axis):
The pressure for each case is obtained by substituting $M_{uy1}$, $M_{uy2}$ and $M_{uyT} = 0$ into equations (1)-(3).

Uniaxial flexure ($R_u$ is located on the X axis):
The pressure for each case is obtained by substituting $M_{ux1}$, $M_{ux2}$ and $M_{uxT} = 0$ into equations (1)-(3).
where: $\sigma_u$, $\sigma_{uP1}$ and $\sigma_{uP2}$ are the ultimate pressures generated by the soil at any point on the footing, $R_u$ (ultimate resultant force) = $P_{u1} + P_{u2}$, $P_{u1}$ and $P_{u2}$ are the ultimate axial loads applied to the footing due to the columns 1 and 2, $(x, y)$, $(x_1, y_1)$, $(x_2, y_2)$ are the coordinates where the ultimate pressure generated by the soil corresponding to the axes of analysis is located, $L_x$ and $L_y$ are the sides of the footing, $M_{uxT}$ (ultimate resultant moment about the X-axis) = $M_{ux1} + M_{ux2} + P_{u1} (L_y/2 - L_{y1}) - P_{u2} (L_y/2 - L_{y2})$, $M_{ux1}$ and $M_{ux2}$ are the moments about the $X_1$ and $X_2$ axes, $M_{uyT}$ (ultimate resultant moment about the Y-axis) = $M_{uy1} + M_{uy2}$, $M_{uy1}$ and $M_{uy2}$ are the moments about the $Y_1$ and $Y_2$ axes, $w_1$ (column 1 analysis width) = $c_{1y} + d$ and $w_2$ (column 2 analysis width) = $c_{2y} + d$.
Equations (1)-(3) or biaxial and uniaxial flexure equations can be applied when the ultimate resultant force $R_u$ is inside the central nucleus (surface in contact with the ground is fully compressed), and when the ultimate resultant force $R_u$ is outside the central nucleus (surface in contact with the ground is partially compressed) these equations are not valid.
When the ultimate resultant force $R_u$ is located outside the central nucleus, the general equations for the pressure generated by the soil below the footing subjected to uniaxial and biaxial flexure are:

Biaxial flexure (Montes-Paramo et al. 2023):
The pressure in the main direction (Y-axis) is:

$$\sigma_{zu}(x,y) = \frac{\sigma_{umax}\left[L_{y3}(2x - L_x) + L_{x3}(2y - L_y) + 2L_{x3}L_{y3}\right]}{2L_{x3}L_{y3}} \tag{4}$$

The pressure in the direction transverse to the main direction (X axis), for $P_{u1}$ on the $X_1$ and $Y_1$ axes (changing coordinates to the center of column 1) is:

$$\sigma_{zuP1}(x_1,y_1) = \frac{\sigma_{umax}\left[L_{y3}(2x_1 - L_x) + 2L_{x3}(y_1 - L_{y1}) + 2L_{x3}L_{y3}\right]}{2L_{x3}L_{y3}} \tag{5}$$

The pressure in the direction transverse to the main direction (X axis), for $P_{u2}$ on the $X_2$ and $Y_2$ axes (changing coordinates to the center of column 2) is:

$$\sigma_{zuP2}(x_2,y_2) = \frac{\sigma_{umax}\left[L_{y3}(2x_2 - L_x) + 2L_{x3}(y_2 - L - L_{y1}) + 2L_{x3}L_{y3}\right]}{2L_{x3}L_{y3}} \tag{6}$$

Uniaxial flexure ($R_u$ is located on the Y axis) (Montes-Páramo et al. 2023):
The pressure in the main direction (Y-axis) is:

$$\sigma_{zu}(x,y) = \frac{\sigma_{umax}\left(2L_{y3} - L_y + 2y\right)}{2L_{y3}} \tag{7}$$

The pressure in the direction transverse to the main direction (X axis), for $P_{u1}$ on the $X_1$ and $Y_1$ axes (changing coordinates to the center of column 1) is:

$$\sigma_{zuP1}(x_1, y_1) = \frac{\sigma_{umax}\left(L_{y3} - L_{y1} + y_1\right)}{L_{y3}} \tag{8}$$

The pressure in the direction transverse to the main direction (X axis), for $P_{u2}$ on the $X_2$ and $Y_2$ axes (changing coordinates to the center of column 2) is:

$$\sigma_{zuP2}(x_2, y_2) = \frac{\sigma_{umax}\left(L_{y3} - L - L_{y1} + y_2\right)}{L_{y3}} \tag{9}$$

Uniaxial flexure ($R_u$ is located on the X axis) (Montes-Páramo et al. 2023):
The pressure in the main direction (Y-axis) is:

$$\sigma_{zu}(x, y) = \frac{\sigma_{umax}(2L_{x3} - L_x + 2x)}{2L_{x3}} \tag{10}$$

The pressure in the direction transverse to the main direction (X axis), for $P_{u1}$ on the $X_1$ and $Y_1$ axes (changing coordinates to the center of column 1) is:

$$\sigma_{zuP1}(x_1, y_1) = \frac{\sigma_{umax}(2L_{x3} - L_x + 2x_1)}{2L_{x3}} \tag{11}$$

The pressure in the direction transverse to the main direction (X axis), for $P_{u2}$ on the $X_2$ and $Y_2$ axes (changing coordinates to the center of column 2) is:

$$\sigma_{zuP2}(x_2, y_2) = \frac{\sigma_{umax}(2L_{x3} - L_x + 2x_2)}{2L_{x3}} \tag{12}$$

where: $\sigma_{umax}$ is the ultimate maximum pressure that the soil must withstand due to the ultimate axial loads and ultimate moments acting on the footing.
The critical sections for moments are located at the faces of the columns and in the interval between the two columns, the flexural shearing are located at a distance $d_p$ (effective depth of the footing) from the faces of the columns, and for the punching shearing they are located in a perimeter formed from a distance $d_p/2$ from the faces of the columns (ACI 318S-19).

## 2.1. RCF under biaxial flexure

Figure 2 represents the 5 possible cases to determine the minimum surface area of a RCF under axial load and two orthogonal moments in each column.
Case I assumes that the entire lower surface of the footing is fully compressed. The pressure exerted by the soil on the footing is determined by equations (1)-(3).
Cases II, III, IV, and V assume that the entire lower surface of the footing is partially compressed; that is, part of the contact surface is not under pressure. The pressure exerted by the soil on the footing is determined by equations (4)-(6).

### *2.1.1. Moments and flexural shearing*

The ultimate moments $M_{ua}$, $M_{ub}$, $M_{uc}$, $M_{ud}$, $M_{ue}$, $M_{uf}$ and $M_{ug}$ appear on the *a-a*, *b-b*, *c-c*, *d-d*, *e-e*, *f-f* and *g-g* axes, and for the ultimate flexural shears $V_{uh}$, $V_{ui}$, $V_{uj}$, $V_{uk}$, $V_{ul}$ y $V_{um}$ appear on the *h-h, i-i*, *j-j*, *k-k*, *l-l* and *m-m* axes.

Figure 3 presents the critical sections of the ultimate moments and ultimate flexural shearing on the X axis for the 5 cases.

**Case I on the X and Y axes**

Figure 3(a) presents the critical sections for case I, and the general equations on the X and Y axes are:

$$V_{ux} = -\int_{y_1}^{\frac{L_y}{2}} \int_{-\frac{L_x}{2}}^{\frac{L_x}{2}} \sigma_u dxdy \tag{13}$$

$V_{uh}$ is obtained by substituting equation (1) and $y_1 = L_{y2} + L + c_{1y}/2 + d - L_y/2$ into equation (13).
$V_{ui}$ is determined by adding $P_{u1}$ and substituting equation (1) and $y_1 = L_{y2} + L - c_{1y}/2 - d - L_y/2$ into equation (13).
$V_{uj}$ is obtained by adding $P_{u1}$ and substituting equation (1) and $y_1 = L_{y2} + c_{2y}/2 + d - L_y/2$ into equation (13).
$V_{uk}$ is determined by adding $R_u$ and substituting equation (1) and $y_1 = L_{y2} - c_{2y}/2 - d - L_y/2$ into equation (13).

$$M_{ux} = -\int_{y_1}^{\frac{L_y}{2}} \int_{-\frac{L_x}{2}}^{\frac{L_x}{2}} \sigma_u (y - y_1) dxdy \tag{14}$$

$M_{ua}$ is obtained by substituting equation (1) and $y_1 = L_{y2} + L + c_{1y}/2 - L_y/2$ into equation (14).
$M_{ub}$ is determined by adding $P_{u1}c_{1y}/2 + M_{ux1}$ and substituting equation (1) and $y_1 = L_{y2} + L - c_{1y}/2 - L_y/2$ into equation (14).
$M_{ud}$ is obtained by adding $P_{u1}(L - c_{2y}/2) + M_{ux1}$ and substituting equation (1) and $y_1 = L_{y2} + c_{2y}/2 - L_y/2$ into equation (14).
$M_{ue}$ is determined by adding $P_{u1}(L + c_{2y}/2) + P_{u2}c_{2y}/2 + M_{ux1} + M_{ux2}$ and substituting equation (1) and y $y_1 = L_{y2} - c_{2y}/2 - L_y/2$ into equation (14).
Adding $P_{u1}(L_y/2 - L_{y1} - y_1) + M_{ux1}$ and substituting equation (1) into equation (14) and developing the integral, and subsequently differentiating with respect to $y_1$ and equating this equation to zero to obtain the point where the moment is maximum, and substituting this point into the same equation to obtain $M_{uc}$ or ultimate maximum moment.

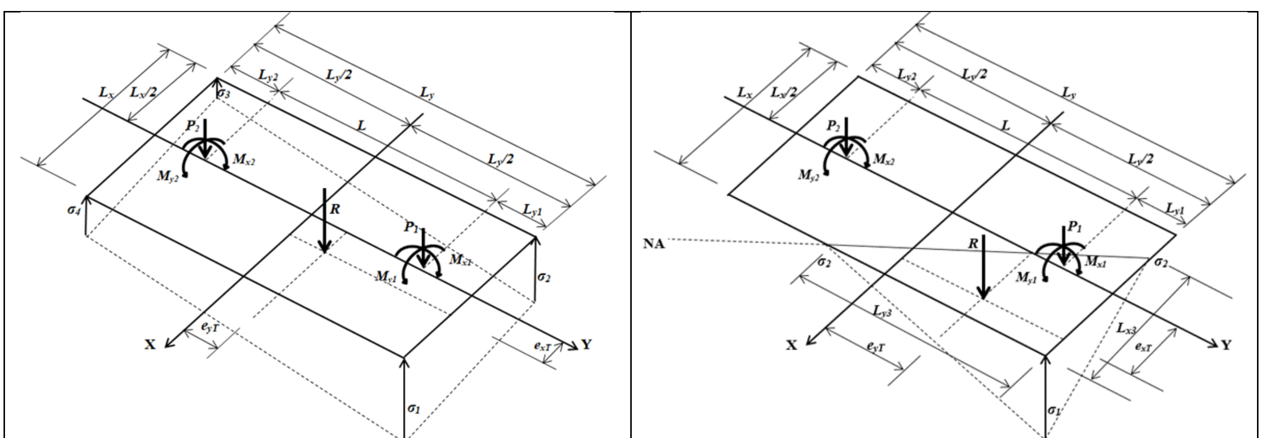


(a) Case I | (b) Case II

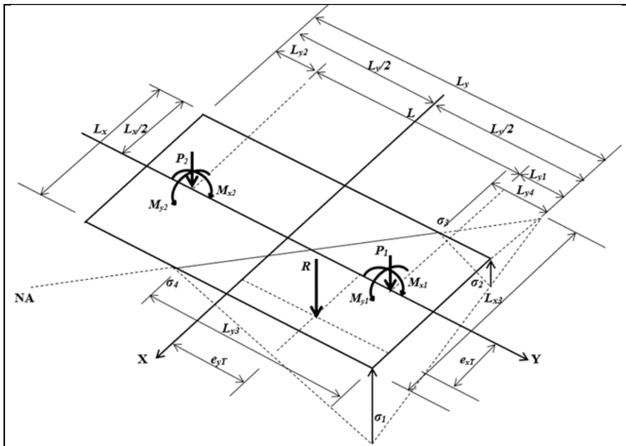

(c) Case III

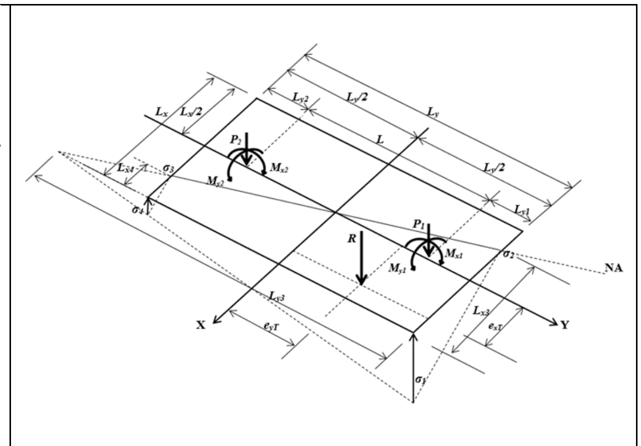

(d) Case IV

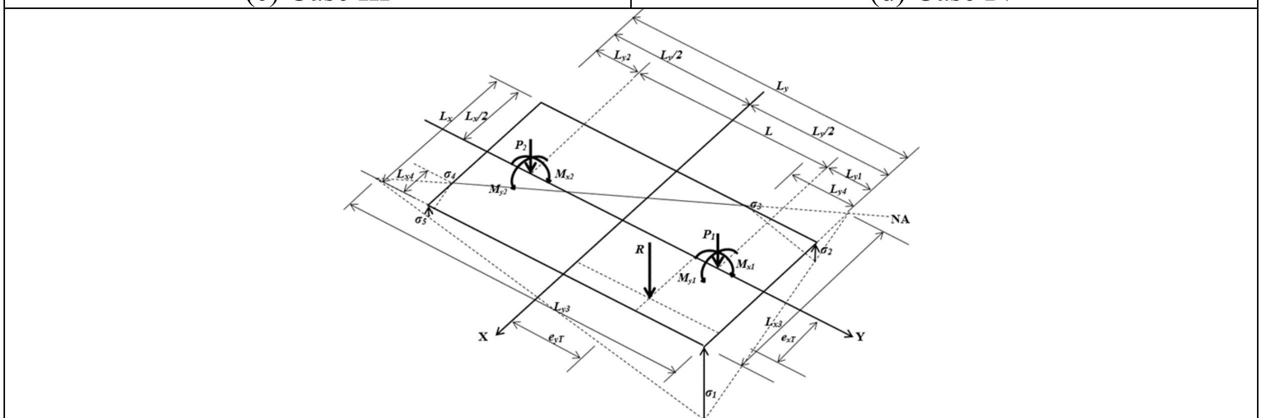

(e) Case V

Figure 2. 5 possible cases for a RCF subjected to biaxial flexure.
Source: Own elaboration based on Montes-Páramo et al. (2023).

The general equations for ultimate flexural shearing and ultimate moments about the Y-axis are:

$$V_{ul} = -\int_{x_1}^{\frac{L_x}{2}} \int_{-\frac{w_1}{2}}^{\frac{w_1}{2}} \sigma_{uP1} dy dx \quad (15)$$

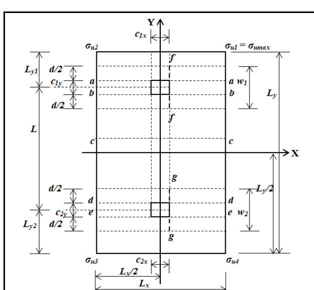

Moments

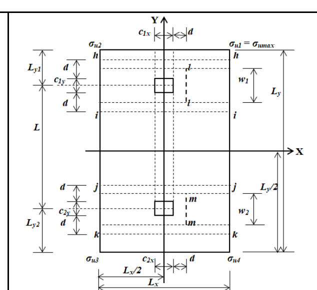

Flexural shearing

(a) Case I

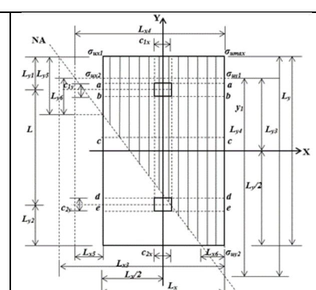

Moments

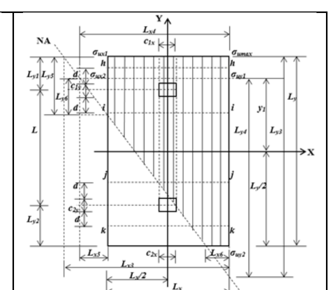

Flexural shearing

(b) Case II

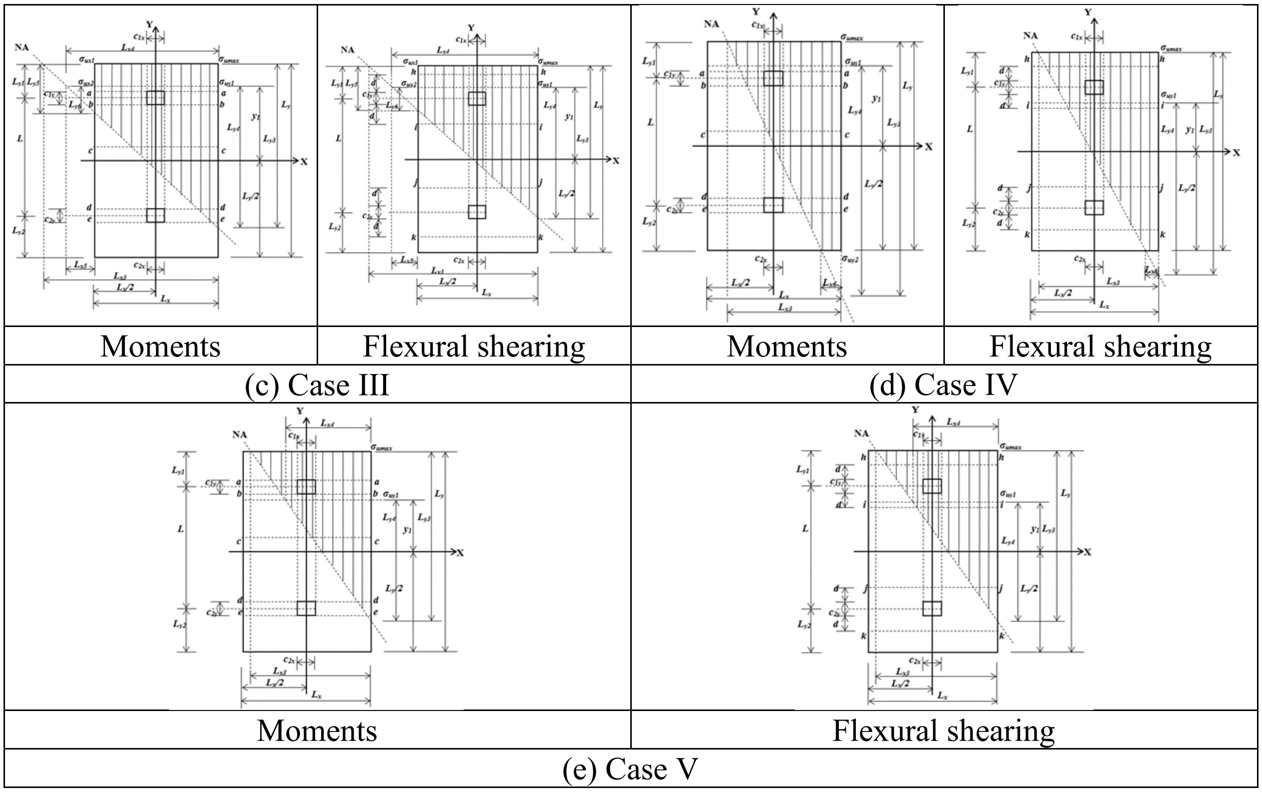


Figure 3. Cases I, II, III, IV and V on the X axis.
Source: Own elaboration.

$V_{ul}$ is obtained by substituting equation (2) and $x_1 = c_{1x}/2 + d$ into equation (15).

$$V_{um} = -\int_{x_2}^{\frac{L_x}{2}} \int_{-\frac{w_2}{2}}^{\frac{w_2}{2}} \sigma_{uP2} dydx \tag{16}$$

$V_{um}$ is determined by substituting equation (3) and $x_2 = c_{2x}/2 + d$ into equation (16).

$$M_{uf} = -\int_{x_1}^{\frac{L_x}{2}} \int_{-\frac{w_1}{2}}^{\frac{w_1}{2}} \sigma_{uP1}(x - x_1) dydx \tag{17}$$

$M_{uf}$ is obtained by substituting equation (2) and $x_1 = c_{1x}/2$ into equation (17).

$$M_{ug} = -\int_{x_2}^{\frac{L_x}{2}} \int_{-\frac{w_2}{2}}^{\frac{w_2}{2}} \sigma_{uP2}(x - x_2) dydx \tag{18}$$

$M_{ug}$ is determined by substituting equation (3) and $x_2 = c_{2x}/2$ into equation (18).

**Case II on the X-axis**

Figure 3(b) presents the critical sections for case II, and the general equations about the X-axis are:
For $L_y/2 \geq y_1 \geq -L_y/2$
When $y_1 \geq L_y/2 - L_{y5} + c_{1y}/2 + d$

$$V_{ux} = -\int_{y_1}^{\frac{L_y}{2}} \int_{-\frac{L_x}{2}}^{\frac{L_x}{2}} \sigma_{zu} dxdy \tag{19}$$

When $y_1 \leq L_y/2 - L_{y5} + c_{1y}/2 + d$

$$V_{ux} = -\int_{\frac{L_y}{2}-L_{y5}}^{\frac{L_y}{2}} \int_{-\frac{L_x}{2}}^{\frac{L_x}{2}} \sigma_z dxdy - \int_{y_1}^{\frac{L_y}{2}-L_{y5}} \int_{\frac{L_x}{2}+\frac{L_{x3}(L_y-2y)}{2L_{y3}}-L_{x3}}^{\frac{L_x}{2}} \sigma_{zu} dxdy \tag{20}$$

where: $L_{y5} = L_{y3}(L_{x3} - L_x)/ L_{x3}$.
$V_{uh}$ is obtained by substituting equation (4) and $y_1 = L_{y2} + L + c_{1y}/2 + d - L_y/2$ into equation (19) or equation (20), as the case may be.
$V_{ui}$ is determined by adding $P_{u1}$ and substituting equation (4) and $y_1 = L_{y2} + L - c_{1y}/2 - d - L_y/2$ into equation (19) or equation (20), as the case may be.
$V_{uj}$ is obtained by adding $P_{u1}$ and substituting equation (4) and $y_1 = L_{y2} + c_{2y}/2 + d - L_y/2$ into equation (19) or equation (20), as the case may be.
$V_{uk}$ is determined by adding $R_u$ and substituting equation (4) and $y_1 = L_{y2} - c_{2y}/2 - d - L_y/2$ into equation (19) or equation (20), as the case may be.
When $y_1 \geq L_y/2 - L_{y5} + c_{1y}/2$

$$M_{ux} = -\int_{y_1}^{\frac{L_y}{2}} \int_{-\frac{L_x}{2}}^{\frac{L_x}{2}} \sigma_{zu}(y - y_1) dxdy \tag{21}$$

When $y_1 \leq L_y/2 - L_{y5} + c_{1y}/2$

$$M_{ux} = -\int_{\frac{L_y}{2}-L_{y5}}^{\frac{L_y}{2}} \int_{-\frac{L_x}{2}}^{\frac{L_x}{2}} \sigma_{zu}(y - y_1) dxdy - \int_{y_1}^{\frac{L_y}{2}-L_{y5}} \int_{\frac{L_x}{2}+\frac{L_{x3}(L_y-2y)}{2L_{y3}}-L_{x3}}^{\frac{L_x}{2}} \sigma_{zu}(y - y_1) dxdy \tag{22}$$

$M_{ua}$ is obtained by substituting equation (4) and $y_1 = L_{y2} + L + c_{1y}/2 - L_y/2$ into equation (21) or equation (22), as the case may be.
$M_{ub}$ is determined by adding $P_{u1}c_{1y}/2 + M_{ux1}$ and substituting equation (4) and $y_1 = L_{y2} + L - c_{1y}/2 - L_y/2$ into equation (21) or equation (22), as the case may be.
$M_{ud}$ is obtained by adding $P_{u1}(L - c_{2y}/2) + M_{ux1}$ and substituting equation (4) and $y_1 = L_{y2} + c_{2y}/2 - L_y/2$ into equation (21) or equation (22), as the case may be.
$M_{ue}$ is determined by adding $P_{u1}(L + c_{2y}/2) + P_{u2}c_{2y}/2 + M_{ux1} + M_{ux2}$ and substituting equation (4) and $y_1 = L_{y2} - c_{2y}/2 - L_y/2$ into equation (21) or equation (22), as the case may be.
Adding $P_{u1}(L_y/2 - L_{y1} - y_1) + M_{ux1}$ and substituting equation (4) into equation (21) or equation (22), as the case may be, and developing the integral, and subsequently differentiating with respect to $y_1$ and equating this equation to zero to obtain the point where the moment is maximum, and substituting this point into the same equation to obtain $M_{uc}$ or ultimate maximum moment.

**Case III on the X axis**
Figure 3(c) represents the critical sections for case III, and the general equations about the X-axis are:
Case III is the same as Case II, but $L_y/2 \geq y_1 \geq L_y/2 - L_{y3}$.

**Case IV on the X axis**
Figure 3(d) indicates the critical sections for case IV, and the general equations about the X-axis are:

For $L_y/2 \geq y_1 \geq - L_y/2$

$$V_{ux} = -\int_{y_1}^{\frac{L_y}{2}} \int_{\frac{L_x}{2}+\frac{L_{x3}(L_y-2y)}{2L_{y3}}-L_{x3}}^{\frac{L_x}{2}} \sigma_{zu} dxdy \tag{23}$$

$V_{uh}$ is obtained by substituting equation (4) and $y_1 = L_{y2} + L + c_{1y}/2 + d - L_y/2$ into equation (23).
$V_{ui}$ is determined by adding $P_{u1}$ and substituting equation (4) and $y_1 = L_{y2} + L - c_{1y}/2 - d - L_y/2$ into equation (23).
$V_{uj}$ is obtained by adding $P_{u1}$ and substituting equation (4) and $y_1 = L_{y2} + c_{2y}/2 + d - L_y/2$ into equation (23).
$V_{uk}$ is determined by adding $R_u$ and substituting equation (4) and $y_1 = L_{y2} - c_{2y}/2 - d - L_y/2$ into equation (23).

$$M_{ux} = -\int_{y_1}^{\frac{L_y}{2}} \int_{\frac{L_x}{2}+\frac{L_{x3}(L_y-2y)}{2L_{y3}}-L_{x3}}^{\frac{L_x}{2}} \sigma_{zu}(y - y_1) dxdy \tag{24}$$

$M_{ua}$ is obtained by substituting equation (4) and $y_1 = L_{y2} + L + c_{1y}/2 - L_y/2$ into equation (24).
$M_{ub}$ is determined by adding $P_{u1}c_{1y}/2 + M_{ux1}$ and substituting equation (4) and $y_1 = L_{y2} + L - c_{1y}/2 - L_y/2$ into equation (24).
$M_{ud}$ is obtained by adding $P_{u1}(L - c_{2y}/2) + M_{ux1}$ and substituting equation (4) and $y_1 = L_{y2} + c_{2y}/2 - L_y/2$ into equation (24).
$M_{ue}$ is determined by adding $P_{u1}(L + c_{2y}/2) + P_{u2}c_{2y}/2 + M_{ux1} + M_{ux2}$ and substituting equation (4) and y $y_1 = L_{y2} - c_{2y}/2 - L_y/2$ into equation (24).
Adding $P_{u1}(L_y/2 - L_{y1} - y_1) + M_{ux1}$ and substituting equation (4) into equation (24) and developing the integral, and subsequently differentiating with respect to $y_1$ and equating this equation to zero to obtain the point where the moment is maximum, and substituting this point into the same equation to obtain $M_{uc}$ or ultimate maximum moment.

**Case V on the X axis**

Figure 3(e) represents the critical sections for case V, and the general equations about the X-axis are:
Case V is the same as Case IV, but $L_y/2 \geq y_1 \geq L_y/2 - L_{y3}$.

**Cases II, III, VI and V on the Y axis**
Figure 4 indicates the critical sections for moments and flexural shearing for cases II, III, IV, and V about the Y-axis.

**Flexural shearing and moments about the Y axis for $P_1$**
**Case A.** When $L_{x4}, L_{x5} \geq L_x/2 - x_1$
where: $L_{x4} = L_{x3}(2L_{y3} - 2L_{y1} + w_1)/2L_{y3}$ and $L_{x5} = L_{x3}(2L_{y3} - 2L_{y1} - w_1)/2L_{y3}$.

$$V_{ul} = -\int_{-\frac{w_1}{2}}^{\frac{w_1}{2}} \int_{x_1}^{\frac{L_x}{2}} \sigma_{zuP1} dxdy \tag{25}$$

$V_{ul}$ is obtained by substituting equation (5) and $x_1 = c_{1x}/2 + d$ into equation (25).

$$M_{uf} = -\int_{-\frac{w_1}{2}}^{\frac{w_1}{2}} \int_{x_1}^{\frac{L_x}{2}} \sigma_{zuP1}(x - x_1) dxdy \tag{26}$$

$M_{uf}$ is obtained by substituting equation (5) and $x_1 = c_{1x}/2$ into equation (26).

**Caso B.** When $L_{x4} \geq L_x/2 - x_1 \geq L_{x5}$

$$V_{ul} = -\int_{L_{y6}}^{\frac{w_1}{2}} \int_{x_1}^{\frac{L_x}{2}} \sigma_{zuP1} dxdy - \int_{-\frac{w_1}{2}}^{L_{y6}} \int_{x_2}^{\frac{L_x}{2}} \sigma_{zuP1} dxdy \tag{27}$$

where: $L_{y6} = L_{y1} + L_{y3}(L_x - 2L_{x3} - 2x_1)/2L_{x3}$ and $x_2 = L_x/2 + L_{x3}(L_{y1} - L_{y3} - y)/L_{y3}$.

$V_{ul}$ is obtained by substituting equation (5) and $x_1 = c_{1x}/2 + d$ into equation (27).

$$M_{uf} = -\int_{L_{y6}}^{\frac{w_1}{2}} \int_{x_1}^{\frac{L_x}{2}} \sigma_{zuP1}(x - x_1) dxdy - \int_{-\frac{w_1}{2}}^{L_{y6}} \int_{x_2}^{\frac{L_x}{2}} \sigma_{zuP1}(x - x_1) dxdy \tag{28}$$

$M_{uf}$ is obtained by substituting equation (5) and $x_1 = c_{1x}/2$ into equation (28).

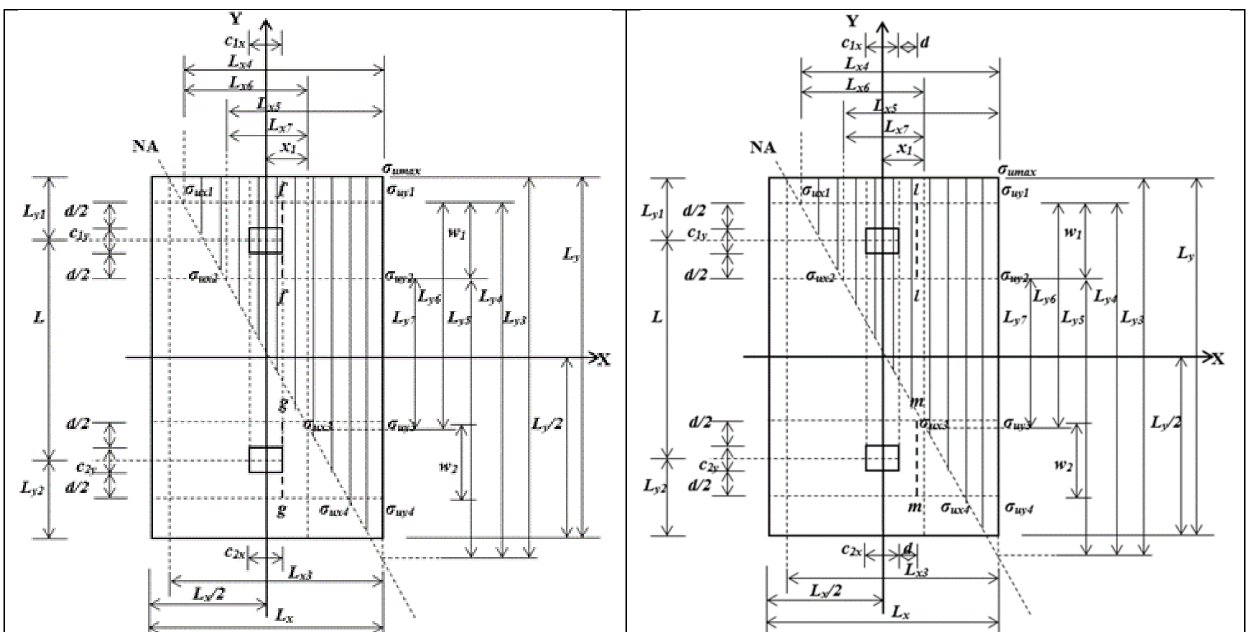


(a) Moments (b) Flexural shearing

Figure 4. Cases II, III, IV and V on the Y axis.
Source: Own elaboration.

**Case C.** When $L_x/2 - x_1 \geq L_{x4}$ and $L_{x5}$

$$V_{ul} = -\int_{-\frac{w_1}{2}}^{\frac{w_1}{2}} \int_{x_2}^{\frac{L_x}{2}} \sigma_{zuP1} dxdy \tag{29}$$

where: $x_2 = L_x/2 + L_{x3}(L_{y1} - L_{y3} - y)/L_{y3}$.
$V_{ul}$ is obtained by substituting equation (5) into equation (29).

$$M_{uf} = -\int_{-\frac{w_1}{2}}^{\frac{w_1}{2}} \int_{x_2}^{\frac{L_x}{2}} \sigma_{zuP1}(x - x_1) dxdy \tag{30}$$

$M_{uf}$ is obtained by substituting equation (5) and $x_1 = c_{1x}/2$ into equation (30).

**Flexural shearing and moments about the Y axis for *P₂***
**Case A.** When $L_{x4}, L_{x5} \geq L_x/2 - x_1$
where: $L_{x4} = L_{x3}(2L_{y3} - 2L_{y1} + w_2)/2L_{y3}$ y $L_{x5} = L_{x3}(2L_{y3} - 2L_{y1} - w_2)/2L_{y3}$.

$$V_{um} = -\int_{-\frac{w_2}{2}}^{\frac{w_2}{2}} \int_{x_1}^{\frac{L_x}{2}} \sigma_{zuP2} dxdy \tag{31}$$

$V_{um}$ is obtained by substituting equation (6) and $x_1 = c_{2x}/2 + d$ into equation (31).

$$M_{ug} = -\int_{-\frac{w_2}{2}}^{\frac{w_2}{2}} \int_{x_1}^{\frac{L_x}{2}} \sigma_{zuP2}(x - x_1) dxdy \tag{32}$$

$M_{ug}$ is obtained by substituting equation (6) and $x_1 = c_{2x}/2$ into equation (32).

**Case B.** When $L_{x4} \geq L_x/2 - x_1 \geq L_{x5}$

$$V_{um} = -\int_{L_{y6}}^{\frac{w_2}{2}} \int_{x_1}^{\frac{L_x}{2}} \sigma_{zuP2} dxdy - \int_{-\frac{w_2}{2}}^{L_{y6}} \int_{x_2}^{\frac{L_x}{2}} \sigma_{zuP2} dxdy \tag{33}$$

where: $L_{y6} = L_{y1} + L_{y3}(L_x - 2L_{x3} - 2x_1)/2L_{x3}$ and $x_2 = L_x/2 + L_{x3}(L_{y1} - L_{y3} - y)/L_{y3}$.

$V_{um}$ is obtained by substituting equation (6) and $x_1 = c_{2x}/2 + d$ into equation (33).

$$M_{ug} = -\int_{L_{y6}}^{\frac{w_2}{2}} \int_{x_1}^{\frac{L_x}{2}} \sigma_{zuP2}(x - x_1) dxdy - \int_{-\frac{w_2}{2}}^{L_{y6}} \int_{x_2}^{\frac{L_x}{2}} \sigma_{zuP2}(x - x_1) dxdy \tag{34}$$

$M_{ug}$ is obtained by substituting equation (6) and $x_1 = c_{2x}/2$ into equation (34).

**Case C.** When $L_x/2 - x_1 \geq L_{x4}$ y $L_{x5}$

$$V_{um} = -\int_{-\frac{w_1}{2}}^{\frac{w_2}{2}} \int_{x_2}^{\frac{L_x}{2}} \sigma_{zuP2} dxdy \tag{35}$$

where: $x_2 = L_x/2 + L_{x3}(L_{y1} - L_{y3} - y)/L_{y3}$.

$V_{um}$ is obtained by substituting equation (6) into equation (35).

$$M_{ug} = -\int_{-\frac{w_2}{2}}^{\frac{w_2}{2}} \int_{x_2}^{\frac{L_x}{2}} \sigma_{zuP2}(x - x_1) dxdy \tag{36}$$

$M_{ug}$ is obtained by substituting equation (6) and $x_1 = c_{2x}/2$ into equation (36).

### *2.1.2. Punching shearing*

The punching shearing $V_{up1}$ and $V_{up2}$ occur in the perimeter formed by points 1, 2, 3 and 4 for column 1, and by points 5, 6, 7 and 8 for column 2.
Figure 5 indicates the critical sections for punching shearing for all cases.

**Case I**

$$V_{up1} = P_{u1} - \int_{\frac{L_y}{2} - L_{y1} - \frac{c_{1y}}{2} - \frac{d}{2}}^{\frac{L_y}{2} - L_{y1} + \frac{c_{1y}}{2} + \frac{d}{2}} \int_{-\frac{c_{1x}}{2} - \frac{d}{2}}^{\frac{c_{1x}}{2} + \frac{d}{2}} \sigma_u dxdy \tag{37}$$

$$V_{up2} = P_{u2} - \int_{\frac{L_y}{2} - L_{y1} - L - \frac{c_{2y}}{2} - \frac{d}{2}}^{\frac{L_y}{2} - L_{y1} - L + \frac{c_{2y}}{2} + \frac{d}{2}} \int_{-\frac{c_{2x}}{2} - \frac{d}{2}}^{\frac{c_{2x}}{2} + \frac{d}{2}} \sigma_u dxdy \tag{38}$$

Substituting equation (1) into equations (37) and (38) yields $V_{up1}$ and $V_{up2}$.

**Case IIA**

$$V_{up1} = P_{u1} - \int_{\frac{L_y}{2} - L_{y1} - \frac{c_{1y}}{2} - \frac{d}{2}}^{\frac{L_y}{2} - L_{y1} + \frac{c_{1y}}{2} + \frac{d}{2}} \int_{-\frac{c_{1x}}{2} - \frac{d}{2}}^{\frac{c_{1x}}{2} + \frac{d}{2}} \sigma_{zu} dxdy \tag{39}$$

$$V_{up2} = P_{u2} - \int_{\frac{L_y}{2} - L_{y1} - L - \frac{c_{2y}}{2} - \frac{d}{2}}^{\frac{L_y}{2} - L_{y1} - L + \frac{c_{2y}}{2} + \frac{d}{2}} \int_{-\frac{c_{2x}}{2} - \frac{d}{2}}^{\frac{c_{2x}}{2} + \frac{d}{2}} \sigma_{zu} dxdy \tag{40}$$

Substituting equation (4) into equations (39) and (40) yields $V_{up1}$ and $V_{up2}$.

**Case IIB**

For $V_{up1}$ is equation (39) and for $V_{up2} = P_{u2}$.

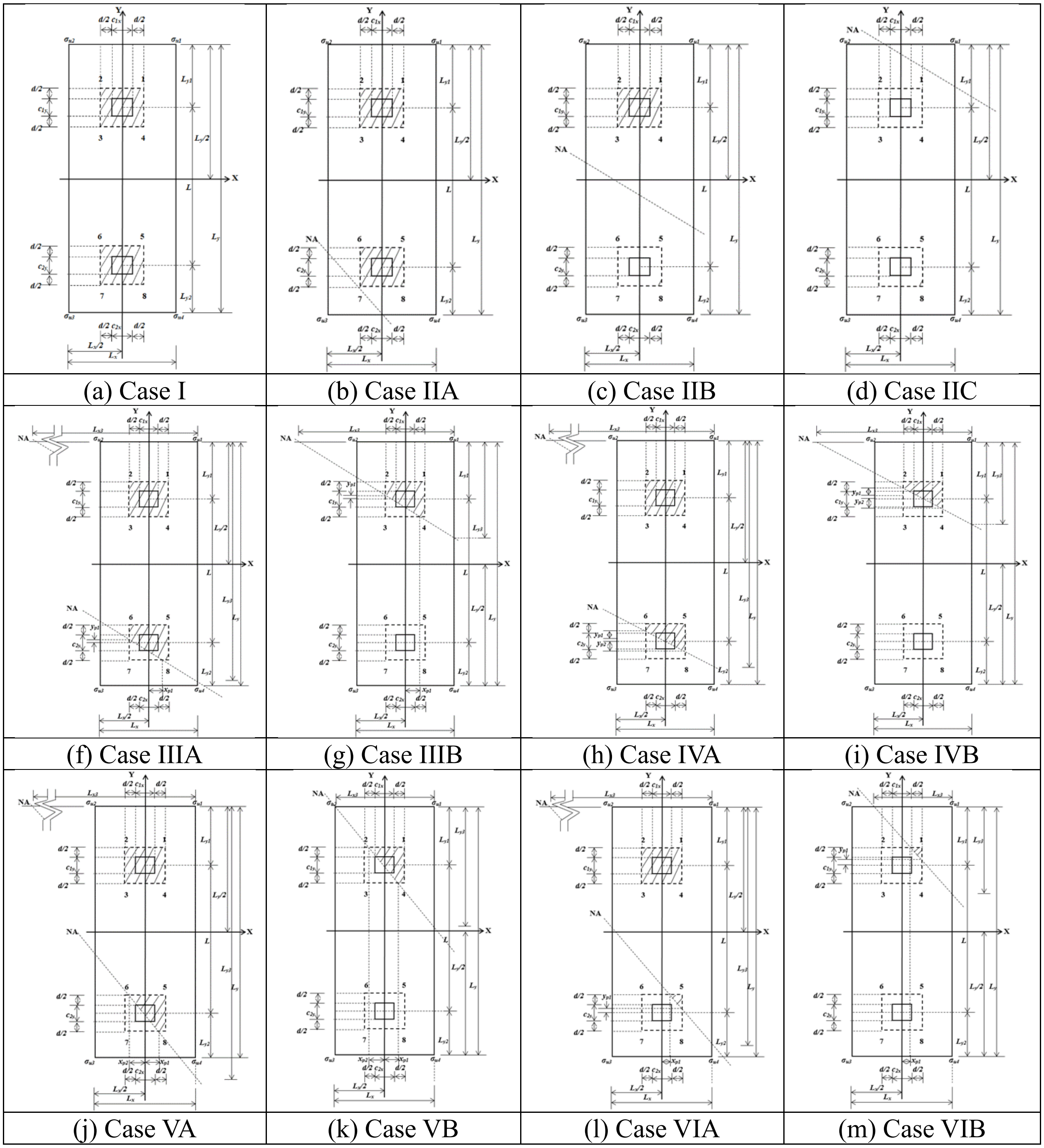

(a) Case I | (b) Case IIA | (c) Case IIB | (d) Case IIC
(f) Case IIIA | (g) Case IIIB | (h) Case IVA | (i) Case IVB
(j) Case VA | (k) Case VB | (l) Case VIA | (m) Case VIB

Figure 5. Punching shearing for biaxial flexure.
Source: Own elaboration.

**Case IIC**
For $V_{up1} = P_{u1}$ and for $V_{up2} = P_{u2}$.

**Caso IIIA**
For $V_{up1}$ is equation (39).

$$V_{up2} = P_{u2} - \int_{-\frac{c_{2x}}{2}-\frac{d}{2}}^{\frac{c_{2x}}{2}+\frac{d}{2}} \int_{\frac{L_y}{2}-\frac{L_{y3}(2x-L_x)}{2L_{x3}}-L_{y3}}^{\frac{L_y}{2}-L_{y1}-L+\frac{c_{2y}}{2}+\frac{d}{2}} \sigma_{uz} dydx - \int_{-\frac{c_{2x}}{2}-\frac{d}{2}}^{x_{p1}} \int_{\frac{L_y}{2}-\frac{L_{y3}(2x-L_x)}{2L_{x3}}-L_{y3}}^{\frac{L_y}{2}-L_{y1}-L+y_{p1}} \sigma_{uz} dydx - \int_{x_{p1}}^{\frac{c_{2x}}{2}+\frac{d}{2}} \int_{\frac{L_y}{2}-L_{y1}-L-\frac{c_{2y}}{2}-\frac{d}{2}}^{\frac{L_y}{2}-L_{y1}-L+y_{p1}} \sigma_{uz} dydx \quad (41)$$

where: $x_{p1} = L_x/2 - L_{x3} + L_{x3}(2L_y - 2L_{y2} + c_{2y} + d)/2L_{y3}$ and $y_{p1} = L_y - L_{y2} - L_{y3} + L_{y3}(L_x + c_{2x} + d)/2L_{x3}$.

**Case IIIB**

$$V_{up1} = P_{u1} - \int_{-\frac{c_{1x}}{2}-\frac{d}{2}}^{\frac{c_{1x}}{2}+\frac{d}{2}} \int_{\frac{L_y}{2}-L_{y1}+y_{p1}}^{\frac{L_y}{2}-L_{y1}+\frac{c_{1y}}{2}+\frac{d}{2}} \sigma_{uz} dydx - \int_{-\frac{c_{1x}}{2}-\frac{d}{2}}^{x_{p1}} \int_{\frac{L_y}{2}-\frac{L_{y3}(2x-L_x)}{2L_{x3}}-L_{y3}}^{\frac{L_y}{2}-L_{y1}+y_{p1}} \sigma_{uz} dydx - \int_{x_{p1}}^{\frac{c_{1x}}{2}+\frac{d}{2}} \int_{\frac{L_y}{2}-L_{y1}-\frac{c_{1y}}{2}-\frac{d}{2}}^{\frac{L_y}{2}-L_{y1}+y_{p1}} \sigma_{uz} dydx \quad (42)$$

where: $x_{p1} = L_x/2 - L_{x3} + L_{x3}(2L_{y1} + c_{1y} + d)/2L_{y3}$ and $y_{p1} = L_{y1} - L_{y3} + L_{y3}(L_x + c_{1x} + d)/2L_{x3}$.
For $V_{up2} = P_{u2}$.

**Case IVA**
For $V_{up1}$ is equation (39).

$$V_{up2} = P_{u2} - \int_{-\frac{c_{2x}}{2}-\frac{d}{2}}^{\frac{c_{2x}}{2}+\frac{d}{2}} \int_{\frac{L_y}{2}-\frac{L_{y3}(2x-L_x)}{2L_{x3}}-L_{y3}}^{\frac{L_y}{2}-L_{y1}-L+\frac{c_{2y}}{2}+\frac{d}{2}} \sigma_{uz} dydx \quad (43)$$

**Case IVB**

$$V_{up1} = P_{u1} - \int_{-\frac{c_{1x}}{2}-\frac{d}{2}}^{\frac{c_{1x}}{2}+\frac{d}{2}} \int_{\frac{L_y}{2}-\frac{L_{y3}(2x-L_x)}{2L_{x3}}-L_{y3}}^{\frac{L_y}{2}-L_{y1}+\frac{c_{1y}}{2}+\frac{d}{2}} \sigma_{uz} dydx \quad (44)$$

For $V_{up2} = P_{u2}$.

**Case VA**
For $V_{up1}$ is equation (39).

$$V_{up2} = P_{u2} - \int_{x_{p1}}^{\frac{c_{2x}}{2}+\frac{d}{2}} \int_{\frac{L_y}{2}-L_{y1}-L-\frac{c_{2y}}{2}-\frac{d}{2}}^{\frac{L_y}{2}-L_{y1}-L+\frac{c_{2y}}{2}+\frac{d}{2}} \sigma_z dydx - \int_{-\frac{c_{2x}}{2}-\frac{d}{2}}^{x_{p1}} \int_{\frac{L_y}{2}-\frac{L_{y3}(2x-L_x)}{2L_{x3}}-L_{y3}}^{\frac{L_y}{2}-L_{y1}-L+\frac{c_{2y}}{2}+\frac{d}{2}} \sigma_z dydx \quad (45)$$

where: $x_{p1} = L_x/2 - L_{x3} + L_{x3}(2L_{y1} + 2L + c_{2y} + d)/2L_{y3}$.

**Caso VB**

$$V_{up1} = P_{u1} - \int_{x_{p1}}^{\frac{c_{1x}}{2}+\frac{d}{2}} \int_{\frac{L_y}{2}-L_{y1}-\frac{c_{1y}}{2}-\frac{d}{2}}^{\frac{L_y}{2}-L_{y1}+\frac{c_{1y}}{2}+\frac{d}{2}} \sigma_z dydx - \int_{-\frac{c_{1x}}{2}-\frac{d}{2}}^{x_{p1}} \int_{\frac{L_y}{2}-\frac{L_{y3}(2x-L_x)}{2L_{x3}}-L_{y3}}^{\frac{L_y}{2}-L_{y1}+\frac{c_{1y}}{2}+\frac{d}{2}} \sigma_z dydx \tag{46}$$

where: $x_{p1} = L_x/2 - L_{x3} + L_{x3}(2L_{y1} + c_{1y} + d)/2L_{y3}$.
For $V_{up2} = P_{u2}$.

**Caso VIA**

For $V_{up1}$ is equation (39)**.**

$$V_{up2} = P_{u2} - \int_{x_{p1}}^{\frac{c_{2x}}{2}+\frac{d}{2}} \int_{\frac{L_y}{2}-\frac{L_{y3}(2x-L_x)}{2L_{x3}}-L_{y3}}^{\frac{L_y}{2}-L_{y1}-L+\frac{c_{2y}}{2}+\frac{d}{2}} \sigma_z dydx \tag{47}$$

where: $x_{p1} = L_x/2 - L_{x3} + L_{x3}(2L_{y1} + 2L - c_{2y} - d)/2L_{y3}$.

**Caso VIB**

$$V_{up1} = P_{u1} - \int_{x_{p1}}^{\frac{c_{1x}}{2}+\frac{d}{2}} \int_{\frac{L_y}{2}-\frac{L_{y3}(2x-L_x)}{2L_{x3}}-L_{y3}}^{\frac{L_y}{2}-L_{y1}+\frac{c_{1y}}{2}+\frac{d}{2}} \sigma_z dydx \tag{48}$$

where: $x_{p1} = L_x/2 - L_{x3} + L_{x3}(2L_{y1} - c_{1y} - d)/2L_{y3}$.
For $V_{up2} = P_{u2}$.

**2.2. RCF under uniaxial flexure**

Figure 6 indicates the four possible cases for determining the minimum surface of a RCF under uniaxial flexure. Two cases when *R* is located on the Y axis: Case Y-I) when *R* is located inside the central nucleus; Case Y-II) when *R* is located outside the central nucleus. Two cases when *R* is located on the X axis: Case X-I) when *R* is located inside the central nucleus; Case X-II) when *R* is located outside the central nucleus.

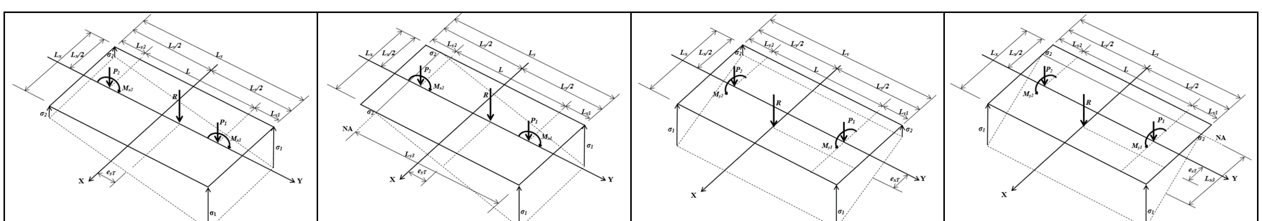

| (a) Case Y-I | (b) Case Y-II | (c) Case X-I | (d) Case X-II |
|---|---|---|---|

Figure 6. Four possible cases for a RCF subjected to uniaxial flexure.
Source: Own elaboration based on Montes-Páramo et al. (2023).

Cases Y-I and X-I assume that the entire lower area of the footing is fully compressed. The pressure exerted by the soil on the footing is determined by equations (1)-(3). But, substituting $M_{uy1}$, $M_{uy2}$ and $M_{uyT} = 0$ for the case Y-I, and $M_{ux1}$, $M_{ux2}$ and $M_{uxT} = 0$ for the case X-I.
Cases Y-II and X-II assume that the entire lower area of the footing is partially compressed, that is, part of the contact area is not under pressure. The pressure exerted by the soil on the footing is determined by equations (7)-(9) for case Y-II, and by equations (10)-(12) for case X-II.

### *2.2.1. Moments and flexural shearing*

The ultimate moments $M_{ua}$, $M_{ub}$, $M_{uc}$, $M_{ud}$, $M_{ue}$, $M_{uf}$ and $M_{ug}$ appear on the *a-a*, *b-b*, *c-c*, *d-d*, *e-e*, *f-f* and *g-g* axes, and for the ultimate flexural shears $V_{uh}$, $V_{ui}$, $V_{uj}$, $V_{uk}$, $V_{ul}$ and $V_{um}$ appear on the *h-h, i-i*, *j-j*, *k-k*, *l-l* and *m-m* axes.
Figure 7 presents the critical sections of the ultimate moments and ultimate flexural shearing for the 4 cases.

**Case Y-I**

Figure 7(a) represents the critical sections for moments and flexural shearing for the case Y-I, and the general equations on the axis X are equations (13) and (14) and on the Y axis are equations (15)-(18), but substituting $M_{uyT} = 0$.

**Case Y-II**

Figure 7(b) represents the critical sections for moments and flexural shearing for the case Y-II, and the general equations about the X axis are equations (19) and (21), but substituting equation (7) instead of equation (4), and the general equations about the Y axis are equations (25) and (26) for $P_{u1}$ and substituting equation (8) instead of equation (5) and equations (31) and (32) for $P_{u2}$ and substituting equation (9) instead of equation (6).

**Case X-I**

Figure 7(c) represents the critical sections for moments and flexural shearing for the case X-I, and the general equations on the axis X are equations (13) and (14) and on the Y axis are equations (15)-(18), but substituting $M_{uxT} = 0$.

**Case X-II**

Figure 7(d) represents the critical sections for moments and flexural shearing for the case X-II, and the general equations about the X axis are equations (19) and (21), but substituting equation (10) instead of equation (4), and the general equations about the Y axis are equations (25) and (26) for $P_{u1}$ and substituting equation (11) instead of equation (5) and equations (31) and (32) for $P_{u2}$ and substituting equation (12) instead of equation (6).

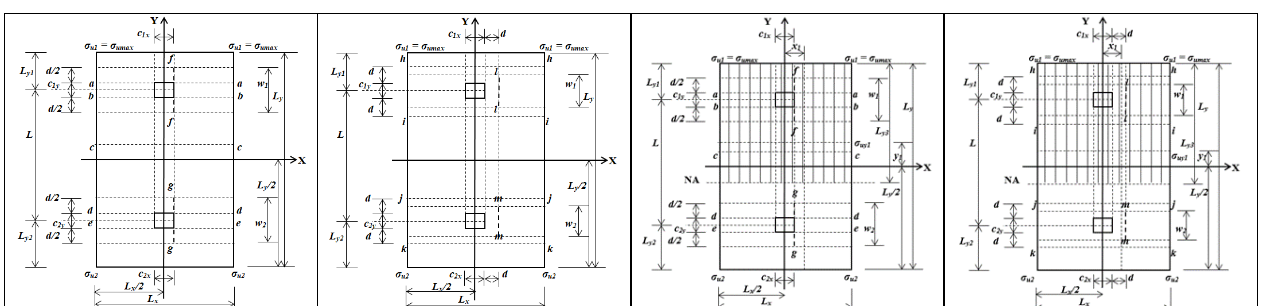

| Moments | Flexural shearing | Moments | Flexural shearing |
|---|---|---|---|
| (a) Case Y-I | | (b) Case Y-II | |

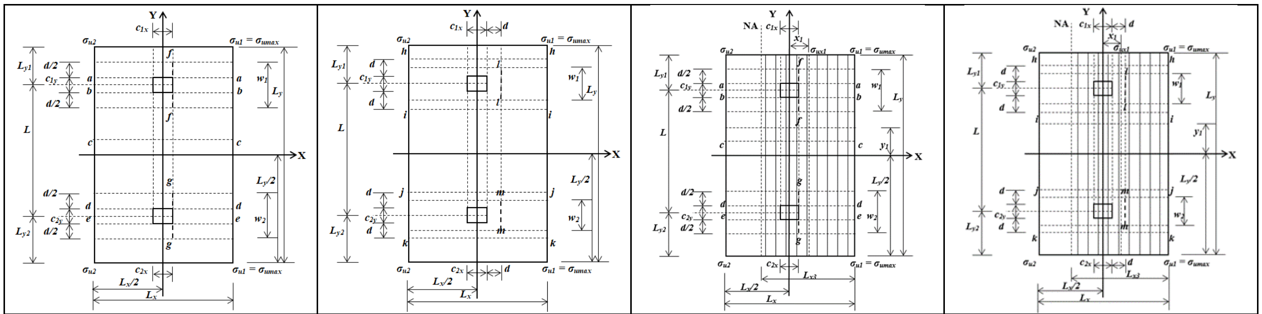

| Moments | Flexural shearing | Moments | Flexural shearing |
|---|---|---|---|
| (c) Case X-I | | (d) Case X-II | |

Figure 7. Cases Y-I, Y-II, X-I and X-II.
Source: Own elaboration.

### *2.2.2. Punching shearing*

The punching shearing $V_{up1}$ and $V_{up2}$ occur in the perimeter formed by points 1, 2, 3 and 4 for column 1, and by points 5, 6, 7 and 8 for column 2.
Figure 8 represents the critical sections for punching shearing for all cases.

**Case Y-I**

The general equations for the ultimate punching shearing are equations (37) and (38), but substituting $M_{uyT} = 0$.

**Case Y-IIA**

For $V_{up1}$ it is equation (39), but substituting equation (7) instead of equation (4).

$$V_{up2} = P_{u2} - \int_{\frac{L_y}{2}-L_{y1}-L+y_{p1}}^{\frac{L_y}{2}-L_{y1}-L+\frac{c_{2y}}{2}+\frac{d}{2}} \int_{-\frac{c_{2x}}{2}-\frac{d}{2}}^{\frac{c_{2x}}{2}+\frac{d}{2}} \sigma_{zu}\, dx\, dy \tag{49}$$

where: $y_{p1} = L_y - L_{y2} - L_{y3}$.

Substituting equation (7) into equation (49) yields $V_{up2}$.

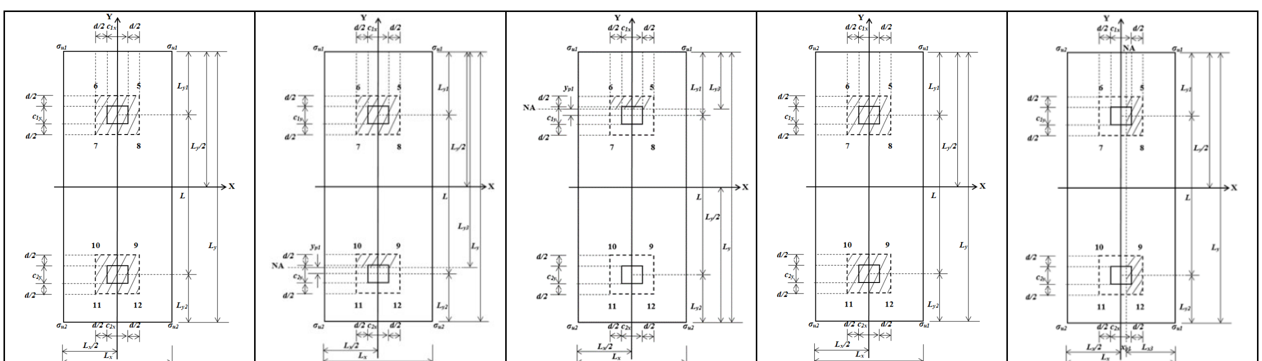

| (a) Case Y-I | (b) Case Y-IIA | (c) Case YII-B | (d) Case X-I | (e) Case X-II |
|---|---|---|---|---|

Figure 8. Punching shearing for uniaxial flexure.
Source: Own elaboration.

**Case Y-IIB**

$$V_{up1} = P_{u1} - \int_{\frac{L_y}{2}-L_{y1}+y_{p1}}^{\frac{L_y}{2}-L_{y1}+\frac{c_{1y}}{2}+\frac{d}{2}} \int_{-\frac{c_{1x}}{2}-\frac{d}{2}}^{\frac{c_{1x}}{2}+\frac{d}{2}} \sigma_{zu}(x,y)dxdy \tag{50}$$

where: $y_{p1} = L_{y1} - L_{y3}$.
Substituting equation (7) into equation (50) yields $V_{up1}$.
For $V_{up2} = P_{u2}$.

**Case X-I**

The general equations for the ultimate punching shearing are equations (37) and (38), but substituting $M_{uxT} = 0$.

**Case X-II**

$$V_{up1} = P_{u1} - \int_{x_{p1}}^{\frac{c_{1x}}{2}+\frac{d}{2}} \int_{\frac{L_y}{2}-L_{y1}-\frac{c_{1y}}{2}-\frac{d}{2}}^{\frac{L_y}{2}-L_{y1}+\frac{c_{1y}}{2}+\frac{d}{2}} \sigma_{zu}dydx \tag{51}$$

$$V_{up2} = P_{u2} - \int_{x_{p1}}^{\frac{c_{2x}}{2}+\frac{d}{2}} \int_{\frac{L_y}{2}-L_{y1}-L-\frac{c_{2y}}{2}-\frac{d}{2}}^{\frac{L_y}{2}-L_{y1}-L+\frac{c_{2y}}{2}+\frac{d}{2}} \sigma_{zu}dydx \tag{52}$$

where: $x_{p1} = L_x/2 - L_{x3}$.
Substituting equation (10) into equations (51) and (52) determines $V_{up1}$ and $V_{up2}$.

## 3. NUMERICAL APPLICATION OF THE PROPOSED MODEL

This section shows the application of the proposed model to justify the advantages of the proposed model against the current model. The data for the examples under biaxial flexure are: The dimensions of the columns are 40x40 cm, $L$ = 6.00 and 7.00 m, and $\sigma_{max}$ = 200 kN/m$^2$, and the footing is subjected to $P_1$ = 500 kN ($P_{D1}$ = 300 kN and $P_{L1}$ = 200 kN), $M_{x1}$ = 1000 kN-m ($M_{xD1}$ = 600 kN-m and $M_{xL1}$ = 400 kN-m), $M_{y1}$ = 250 kN-m ($M_{yD1}$ = 150 kN-m and $M_{yL1}$ = 100 kN-m), $P_2$ = 1000 kN ($P_{D2}$ = 600 kN and $P_{L2}$ = 400 kN), $M_{x2}$ = 2000 kN-m ($M_{xD2}$ = 1200 kN-m and $M_{xL2}$ = 800 kN-m), $M_{y2}$ = 500 kN-m ($M_{yD2}$ = 300 kN-m and $M_{yL2}$ = 200 kN-m), for the four types of constraints in the Y-axis direction (without constraints, limited in column 1, limited in column 2, limited in both columns) (see Figure 9). The minimum area and sides of the RCF for the four types of constraints; these coincide in two types (no constraints and limited in column 2) and the other two types (limited in column 1 and limited in both columns); this is shown in the document proposed by Montes-Páramo et al., (2023). Now, according to the code (ACI 318S-19), the ultimate loads and moments are obtained as follows: $U = 1.2D + 1.6L$ ($U$ is the ultimate load or ultimate moment, $D$ is the dead load or dead load moment, $L$ is the live load or live load moment). The ultimate loads and ultimate moments will be: $P_{u1}$ = 680 kN, $M_{ux1}$ = 1360 kN-m, $M_{uy1}$ = 340 kN-m, $P_{u2}$ = 1360 kN, $M_{ux2}$ = 2720 kN-m, $M_{uy2}$ = 680 kN-m, $\sigma_{umax}$ = 272 kN/m$^2$, the ultimate maximum pressure is obtained from the known dimensions and using the ultimate loads and ultimate moments by equations (12) to (14) of Montes-Páramo et al., (2023).

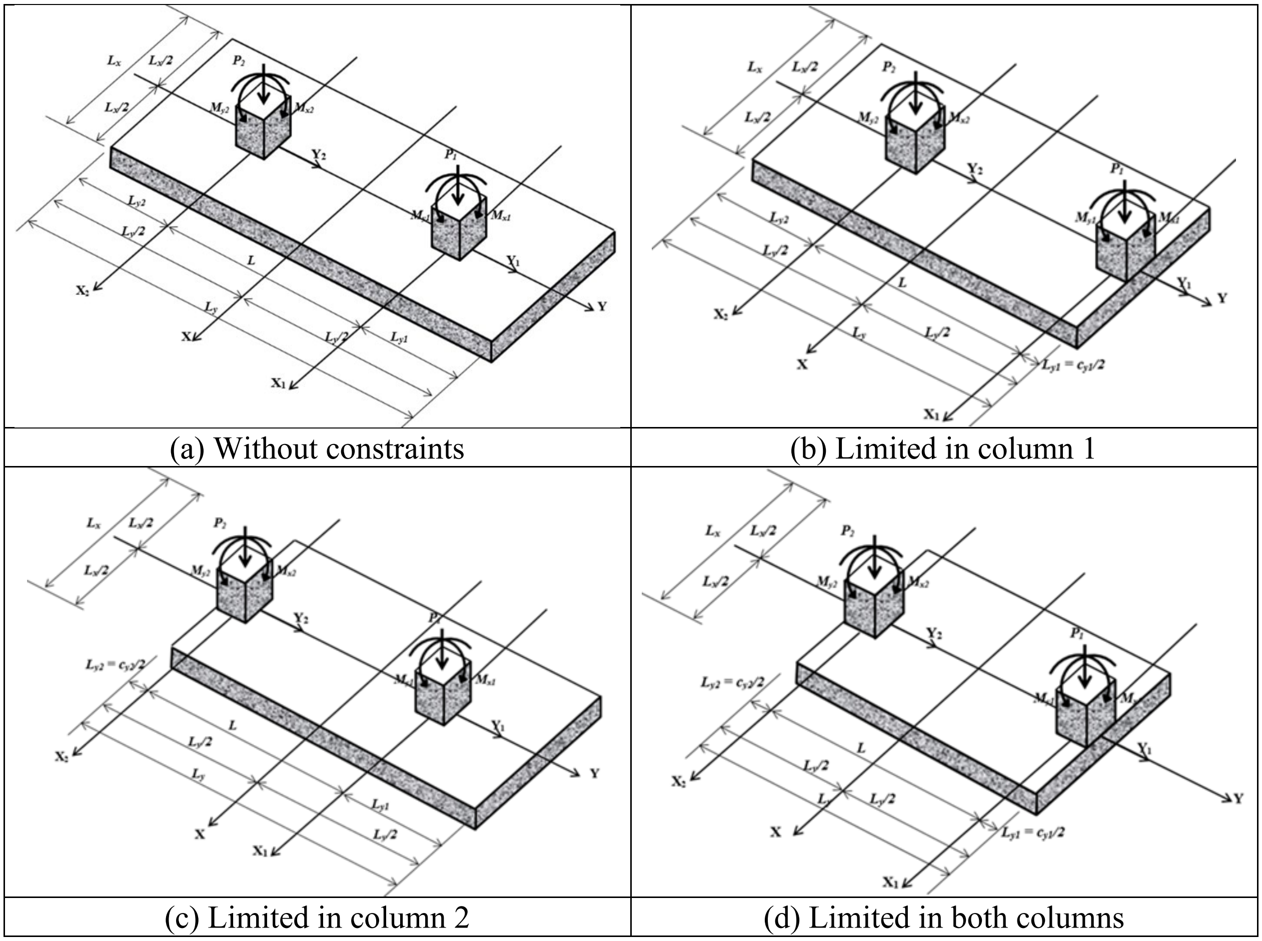

(a) Without constraints | (b) Limited in column 1

(c) Limited in column 2 | (d) Limited in both columns

Figure 9. Four types of constraints in the Y-axis direction.
Source: Own elaboration.

For all examples, $f'_c$ (concrete strength at 28 days) = 21 MPa, $f_y$ (steel strength at yield point) = 420 MPa and $r$ (concrete cover) = 8 cm are used.
Table 1 shows in detail the complete design of the RCFs under biaxial flexure (see Annex).
The data for the examples under uniaxial flexure for both cases are:
1) When the loads are located on the Y axis (Case Y): the dimensions of the columns are 40x40 cm, $L$ = 6.00 and 7.00 m and $\sigma_{max}$ = 200 kN/m$^2$, and the footing is subjected to $P_1$ = 500 kN ($P_{D1}$ = 300 kN and $P_{L1}$ = 200 kN), $M_{x1}$ = 1000 kN-m ($M_{xD1}$ = 600 kN-m and $M_{xL1}$ = 400 kN-m), $M_{y1}$ = 0 kN-m ($M_{yD1}$ = 0 kN-m and $M_{yL1}$ = 0 kN-m), $P_2$ = 500 kN ($P_{D2}$ = 300 kN and $P_{L2}$ = 200 kN), $M_{x2}$ = 2000 kN-m ($M_{xD2}$ = 1200 kN-m and $M_{xL2}$ = 800 kN-m), $M_{y2}$ = 0 kN-m ($M_{yD2}$ = 0 kN-m and $M_{yL2}$ = 0 kN-m). The ultimate loads and ultimate moments will be: $P_{u1}$ = 680 kN, $M_{ux1}$ = 1360 kN-m, $M_{uy1}$ = 0 kN-m, $P_{u2}$ = 680 kN, $M_{ux2}$ = 2720 kN-m, $M_{uy2}$ = 0 kN-m, $\sigma_{umax}$ = 272 kN/m$^2$, the ultimate maximum pressure is obtained using the ultimate loads and ultimate moments from equations (32) and (33) of Montes-Páramo et al., (2023).
2) When the loads are located on the X axis (Case X): the dimensions of the columns are 40x40 cm, $L$ = 6.00 and 7.00 m and $\sigma_{max}$ = 200 kN/m$^2$, and the footing is subjected to $P_1$ = 500 kN ($P_{D1}$ = 300 kN and $P_{L1}$ = 200 kN), $M_{x1}$ = 0 kN-m ($M_{xD1}$ = 0 kN-m and $M_{xL1}$ = 0 kN-m), $M_{y1}$ = 1000 kN-m ($M_{yD1}$ = 600 kN-m and $M_{yL1}$ = 400 kN-m), $P_2$ = 500 kN ($P_{D2}$ = 300 kN and $P_{L2}$ = 200 kN), $M_{x2}$ = 0 kN-m ($M_{xD2}$ = 0 kN-m and $M_{xL2}$ = 0 kN-m), $M_{y2}$ = 2000 kN-m ($M_{yD2}$ = 1200 kN-m and $M_{yL2}$ = 800 kN-m). The ultimate loads and ultimate moments will be: $P_{u1}$ = 680 kN, $M_{ux1}$ = 0 kN-m, $M_{uy1}$ = 1360 kN-m, $P_{u2}$ = 680 kN, $M_{ux2}$ = 0 kN-m, $M_{uy2}$ = 2720 kN-m, $\sigma_{umax}$ = 272 kN/m$^2$, the ultimate

maximum pressure is obtained using the ultimate loads and ultimate moments from equations (41) and (42) of Montes-Páramo et al., (2023).
The minimum area and sides of the RCFs are shown in the document proposed by Montes-Páramo et al., (2023).
Table 2 shows in detail the complete design of the RCFs under uniaxial flexure (see Annex).

# 4. RESULTS

## 4.1 Verification of the equations for the complete design of the RCFs subjected to biaxial flexure

### *4.1.1 Current model or Case I*

For moments: Substituting $y_1 = L_y/2$ into equation (14), the moment is determined as $M_{uao} = 0$ (moment at the end of the footing on the column side 1), now adding $P_{u1}(L + L_{y2}) + P_{u2}L_{y2} + M_{ux1} + M_{ux2}$ and substituting $y_1 = -L_y/2$ into equation (14), the moment is obtained as $M_{ueo} = 0$ (moment at the end of the footing on the column side 2).
For flexural shearing: Substituting $y_1 = L_y/2$ into equation (13), the flexural shearing is determined as $V_{uho} = 0$ (flexural shearing at the end of the footing on the column side 1), now adding $P_{u1} + P_{u2}$ and substituting $y_1 = -L_y/2$ into equation (13), the flexural shearing is obtained $V_{uko} = 0$ (flexural shearing at the end of the footing on the column side 2).

### *4.1.2 New Model or Case II, III, IV and V*

For moments: Substituting $y_1 = L_y/2$ into equation (21) or (22) (cases II and III) and into equation (24) (cases IV and V), as appropriate, the moment is determined as $M_{uao} = 0$ (moment at the end of the footing on the column side 1), now adding $P_{u1}(L + L_{y2}) + P_{u2}L_{y2} + M_{ux1} + M_{ux2}$ and substituting $y_1 = -L_y/2$ into equation (21) or (22) (cases II and III) and into equation (24) (cases IV and V), as appropriate, the moment is obtained as $M_{ueo} = 0$ (moment at the end of the footing on the column side 2).
For flexural shearing: Substituting $y_1 = L_y/2$ into equation (19) or (20) (cases II and III) and into equation (23) (cases IV and V), as appropriate, the flexural shearing is determined as $V_{uho} = 0$ (flexural shearing at the end of the footing on the column side 1), now adding $P_{u1} + P_{u2}$ and substituting $y_1 = -L_y/2$ into equation (19) or (20) (cases II and III) and into equation (23) (case IV), as appropriate, the flexural shearing is obtained as $V_{uko} = 0$ (flexural shearing at the end of the footing on the column side 2).

## 4.2 Verification of the equations for the complete design of RCFs subjected to uniaxial flexure

### *4.2.1 Current model or Cases Y-I and X-I*

The equations are the same as those for biaxial flexure, but taking into account $M_{uyT} = 0$ or $M_{uxT} = 0$ as the case may be.

### *4.2.2 New Model or Cases Y-II and X-II*

The equations are the same as those for biaxial flexure, but taking into account equation (21) for moment and equation (19) for flexural shearing and $M_{uyT} = 0$ or $M_{uxT} = 0$ as the case may be.

## 4.3 Results and Discussion

Table 1 shows the following (see Annex):
For footings with both ends free and constrained at $L_{y2}$:
The thickness is governed by the flexural shearing at $V_{um}$ for case I and at $V_{uj}$ for case IV at $L$ = 6.00 and 7.00 m.

The proposed steel areas in the Y-axis direction: $A_{spyN}$ is governed by the steel provided by the negative moment for both cases, and $A_{spyP}$ is governed by the minimum steel $A_{sminy}$ for both cases at $L$ = 6.00 and 7.00 m.
The proposed steel areas in the X-axis direction: $A_{spxw1}$ and $A_{spxw2}$ are governed by the minimum steel $A_{sminxw1}$ and $A_{sminxw2}$ for cases I and IV at $L$ = 6.00 and 7.00 m.
For footings with both ends constrained and constrained at $L_{y1}$:
The thickness is governed by moment at $M_{ug}$ for case I and the flexural shearing at $V_{uj}$ for case II at $L$ = 6.00 m, and by the flexural shearing at $V_{um}$ for case I and at $V_{uj}$ for case II at $L$ = 7.00 m.
The proposed steel areas in the Y-axis direction: $A_{spyN}$ and $A_{spyP}$ are governed by the minimum steel $A_{sminy}$ for case I at $L$ = 6.00 and 7.00 m, $A_{spyN}$ and $A_{spyP}$ are governed by the steel provided by the negative moment for case II at $L$ = 6.00 and 7.00 m.
The proposed steel areas in the X-axis direction: $A_{spxw1}$ is governed by the minimum steel $A_{sminxw1}$ below column 1 for cases I and II, except for case I at $L$ = 6.00 m. The proposed steel areas in the X-axis direction: $A_{spxw2}$ is governed by the steel provided for the negative moment below column 2 for cases I and II, except for case II at $L$ = 7.00 m.
Table 2 shows the following (see Annex):
For footings under uniaxial flexure (Case Y) (see Annex):
The thickness is governed by the flexural shearing at $V_{uj}$ for cases Y-1 and Y-II at $L$ = 6.00 and 7.00 m.
The proposed steel areas in the Y-axis direction: $A_{spyN}$ is governed by the steel provided by the negative moment and $A_{spyP}$ is governed by the minimum steel $A_{sminy}$ for cases Y-1 and Y-II at $L$ = 6.00 and 7.00 m.
The proposed steel areas in the X-axis direction: $A_{spxw1}$ is governed by the minimum steel $A_{sminxw1}$ for cases Y-1 and Y-II at $L$ = 6.00 and 7.00 m and for $A_{spxw2}$ the same occurs as in $A_{spxw1}$.
For footings under uniaxial flexure (Case X) (see Annex):
The thickness is governed by the flexural shearing at $V_{um}$ for case X-1 at $L$ = 6.00 and 7.00 m, and for X-II is governed by the flexural shearing at $V_{ul}$ and $V_{um}$.
The proposed steel areas in the Y-axis direction: $A_{smyN}$ and $A_{spyP}$ are governed by the minimum steel $A_{sminy}$ for cases X-1 and X-II at $L$ = 6.00 and 7.00 m.
The proposed steel areas in the X-axis direction: $A_{spxw1}$ is governed by the steel provided by the moment under column 1 for cases X-1 and X-II at $L$ = 6.00 and 7.00 m, and for $A_{spxw2}$ the same occurs as in $A_{spxw1}$.
Figure 10 shows in detail the general design (dimensions and reinforcing steel) for RCFs.
Figure 11 represents the volumes of concrete and steel for biaxial flexure for the four types of constraints.
Figure 11(a) shows the concrete volumes for biaxial flexure. The largest volumes are for the current model for all types of constraints, and the largest occurs at $L$ = 6.00 m, which is 29.72 times the current model with respect to the proposed model for the constrained sides at $L_{y1}$ and $L_{y2}$, and for the constrained side at $L_{y1}$.
Figure 11(b) shows the steel volumes for biaxial flexure. The largest volumes are for the current model for all types of constraints, and the largest occurs at $L$ = 6.00 m, which is 28.74 times the current model with respect to the proposed model for the constrained sides at $L_{y1}$ and $L_{y2}$, and for the constrained side at $L_{y1}$.
The volumes of concrete and steel are determined as follows: $V_c = L_xL_yt - (A_{spyN} + A_{spyP})L_y - (A_{spxw1} + A_{spxw2} + A_{sti} + A_{sts})L_x$ and $V_s = (A_{spyN} + A_{spyP})L_y + (A_{spxw1} + A_{spxw2} + A_{sti} + A_{sts})L_x$. The length of the hook is not considered here because the total length of the footing bars is equivalent to the total length with the hook, since the cover and the development of the hook would have to be subtracted.

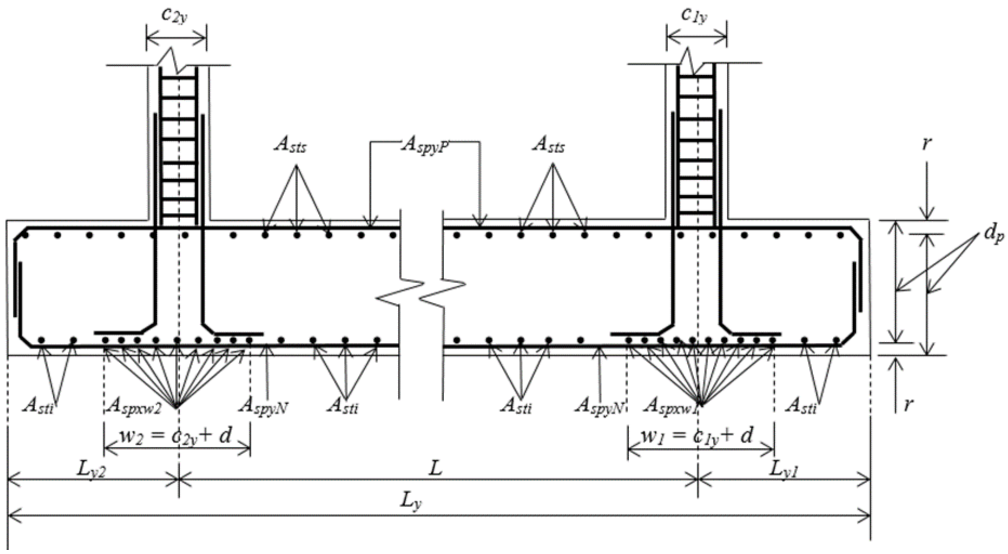


Figure 10. General design for RCFs.
Source: Own elaboration.

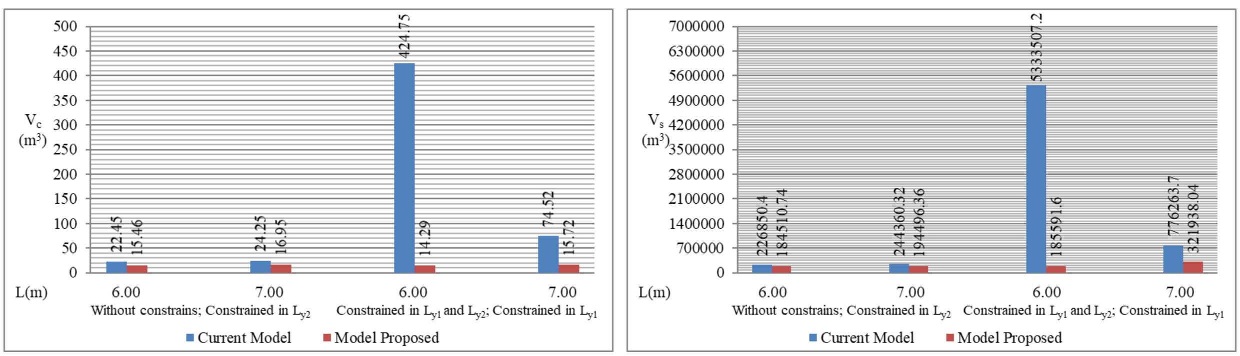


(a) Volume of concrete (b) Volume of steel
Figure 11. Volumes of concrete and steel for biaxial flexure.
Source: Own elaboration.

Figure 12 shows the volumes of concrete and steel for uniaxial flexure for the two cases X and Y. Figure 12(a) shows the concrete volumes for uniaxial flexure. The volume for case Y is slightly larger in the current model at $L$ = 7.00 m compared to the proposed model, and the proposed model is larger at $L$ = 6.00 m, which is 1.56 times the current model. The largest volume in case X is for the current model, and the largest appears at $L$ = 6.00 m at 6.53 times and the smallest appears at $L$ = 7.00 m at 5.79 times the current model with respect to the proposed model.
Figure 12(b) shows the steel volumes for uniaxial flexure. The volume for case Y is slightly larger in the current model at $L$ = 7.00 m compared to the proposed model, and the proposed model is larger at $L$ = 6.00 m, which is 1.06 times the current model. The largest volume in case X is for the current model, and the largest appears at $L$ = 6.00 m at 6.88 times and the smallest appears at $L$ = 7.00 m at 5.81 times the current model with respect to the proposed model.

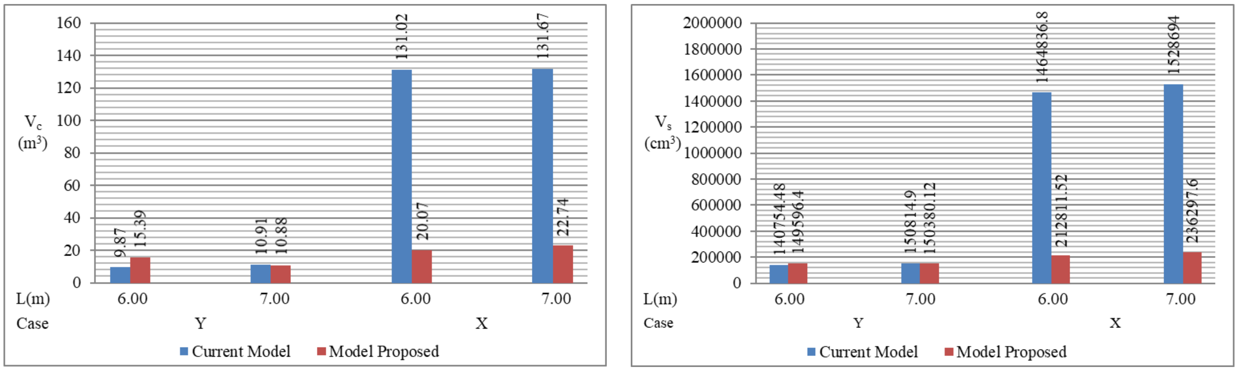


(a) Volume of concrete (b) Volume of steel

Figure 12. Volumes of concrete and steel for uniaxial flexure.
Source: Own elaboration.

Furthermore, a comparison is made between the PM (proposed model) and the PE (practical example) proposed by Luévanos-Rojas (2016a) (restricted sides in the Y direction or longitudinal direction), where the data of the example under biaxial bending are: The dimensions of the columns are 40x40 cm, $L_{y1}$ = 0.20 m, $L_{y2}$ = 0.20 m, $L$ = 5.60 m, $L_y$ = 6.00 m y $\sigma_{max}$ = 220 kN/m$^2$, and the footing is subjected to $P_1$ = 1000 kN ($P_{D1}$ = 600 kN and $P_{L1}$ = 400 kN), $M_{x1}$ = 240 kN-m ($M_{xD1}$ = 140 kN-m and $M_{xL1}$ = 100 kN-m), $M_{y1}$ = 200 kN-m ($M_{yD1}$ = 120 kN-m and $M_{yL1}$ = 80 kN-m), $P_2$ = 800 kN ($P_{D2}$ = 500 kN and $P_{L2}$ = 300 kN), $M_{x2}$ = 220 kN-m ($M_{xD2}$ = 120 kN-m and $M_{xL2}$ = 100 kN-m), $M_{y2}$ = 200 kN-m ($M_{yD2}$ = 110 kN-m and $M_{yL2}$ = 90 kN-m). The ultimate loads and ultimate moments will be: $P_{u1}$ = 1360 kN, $M_{ux1}$ = 328 kN-m, $M_{uy1}$ = 272 kN-m, $P_{u2}$ = 1080 kN, $M_{ux2}$ = 304 kN-m, $M_{uy2}$ = 272 kN-m, $R_u$ = 2440 *kN;* $M_{uyT}$ = 548 kN-m, $M_{uxT}$ = 1416 kN-m, $\sigma_{umax}$ = 299.42 kN/m$^2$, the ultimate maximum pressure is determined using the ultimate loads and ultimate moments from equation (7) of Montes-Páramo et al., (2023).
Table 3 represents in detail the comparison of the final dimensions between the PM (case II) and the PE (case I).

Table 3. Comparison of the final dimensions between the PM and the PE.
(Source: Own elaboration)

| Model | $d_p$ (m) | $t$ (cm) | $L$ (m) | $L_x$ (m) | $L_y$ (m) | $L_{y1}$ (m) | $L_{y2}$ (m) | $L_{x3}$ (m) | $L_{y3}$ (m) | $A_{min}$ (m$^2$) |
|---|---|---|---|---|---|---|---|---|---|---|
| PM | 52 | 60 | 5.60 | 2.80 | 6.00 | 0.20 | 0.20 | 5.91 | 10.87 | 16.80 |
| PE | 77 | 85 | 5.60 | 3.30 | 6.00 | 0.20 | 0.20 | - | - | 19.80 |

where: $t$ is the total thickness, $A_{min}$ is the minimum plan area of the footing.

Table 3 shows that PM is less than PE for $L_x$ and $A_{min}$.
Table 4 represents in detail the comparison of the ultimate moments for design in each section between the PM and the PE.

Table 4. Comparison of the ultimate moments for design between the PM and the PE.
(Source: Own elaboration)

| Model | $M_{ua}$ (kN-m) | $M_{ub}$ (kN-m) | $M_{uc}$ (kN-m) | $M_{ud}$ (kN-m) | $M_{ue}$ (kN-m) | $Ø_fM_{ux}$ (kN-m) | $M_{uf}$ (kN-m) | $Ø_fM_{uf}$ *(kN-m)* | $M_{ug}$ (kN-m) | $Ø_fM_{ug}$ *(kN-m)* |
|---|---|---|---|---|---|---|---|---|---|---|
| PM | 0 | 549.65 | 1223.14 | -100.74 | 0 | 3703.84 | -139.67 | 873.05 | --66.36 | 873.05 |
| PE | 0 | 549.43 | 1652.53 | -102.49 | 0 | 9571.55 | -544.64 | 2276.87 | -457.08 | 2276.87 |

where: $M_{ua}$ is the moment acting on axis $a$, $M_{ub}$ is the moment acting on axis $b$, $M_{uc}$ is the maximum positive moment, $M_{ud}$ is the moment acting on axis $d$, $M_{ue}$ is the moment acting on axis $e$, $Ø_f$

(reduction factor of flexural strength) = 0.90, $Ø_f M_{ux}$ is the resisting moment in the direction parallel to the X axis, $M_{uf}$ is the moment acting on axis $f$, $Ø_f M_{uf}$ is the resisting moment on axis $f$, $M_{ug}$ is the moment acting on axis $g$, $Ø_f M_{ug}$ is the resisting moment on axis $g$.

Table 4 shows that PM is less than PE for all ultimate moments, except for $M_{ub}$.

Table 5 represents in detail the comparison of the ultimate flexural shearing for design in each section between the PM and the PE.

Table 5. comparison of the ultimate flexural shearing for design between the PM and the PE. (Source: Own elaboration)

| Model | $V_{uh}$ (kN) | $V_{ui}$ (kN) | $V_{uj}$ (kN) | $V_{uk}$ (kN) | $Ø_v V_{ux}$ (kN) | $V_{ul}$ (kN) | $Ø_v V_{uy}$ (kN) | $V_{um}$ (kN) | $Ø_v V_{uy}$ (kN) |
|---|---|---|---|---|---|---|---|---|---|
| **PM** | 0 | 613.28 | -893.73 | 0 | 964.14 | -131.91 | 227.26 | -62.67 | 227.26 |
| **PE** | 0 | 661.92 | -826.48 | 0 | 1682.60 | -361.15 | 400.26 | -304.64 | 400.26 |

where: $V_{uh}$ is the flexural shearing about axis $h$, $V_{ui}$ is the flexural shearing about axis $i$, $V_{uj}$ is the flexural shearing about axis $j$, $V_{uk}$ is the flexural shearing about axis $k$, $Ø_v$ (shear resistance reduction factor) = 0.85, $Ø_v V_{ux}$ is the flexural shearing that the concrete resists in the direction parallel to the X axis, $V_{ul}$ is the flexural shear about axis $l$, $Ø_v V_{ul}$ is the flexural shear that the concrete resists about axis $l$, $V_{um}$ is the flexural shearing about axis $m$, $Ø_v V_{um}$ is the flexural shearing that the concrete resists about axis $m$.

Table 5 indicates that PM is less than PE for all ultimate flexural shearing, except for $V_{uj}$ in absolute value.
Table 6 represents in detail the comparison of the ultimate punching shearing for design in each section between the PM and the PE.

Table 6. Comparison of the ultimate punching shearing for design between the PM and the PE. (Source: Own elaboration)

| Model | $V_{up1}$ (kN) | $Ø_v V_{upR11}$ (kN) | $Ø_v V_{upR12}$ (kN) | $Ø_v V_{upR13}$ (kN) | $V_{up2}$ (kN) | $Ø_v V_{upR21}$ (kN) | $Ø_v V_{upR22}$ (kN) | $Ø_v V_{upR23}$ (kN) |
|---|---|---|---|---|---|---|---|---|
| **PM** | 1226.80 | 7214.02 | 3375.78 | 1497.25 | 1036.12 | 7214.02 | 3375.78 | 1497.25 |
| **PE** | 1189.73 | 13066.73 | 7114.75 | 2711.96 | 1023.66 | 13066.73 | 7114.75 | 2711.96 |

where: $V_{up1}$ is the punching shearing acting on column 1; $Ø_v V_{upR12}$, $Ø_v V_{upR22}$ and $Ø_v V_{upR13}$ are the punching shearing that the concrete resists in column 1; $Ø_v V_{up2}$ is the punching shearing acting on column 2; $Ø_v V_{upR21}$, $Ø_v V_{upR22}$ and $Ø_v V_{upR23}$ are the punching shearing that the concrete resists in column 2.

Table 6 shows that PM is greater than PE for all ultimate punching shearing acting on the footing, but for the ultimate punching shearing that the concrete resists, PM is less than PE.
Table 7 shows in detail the comparison of the steel areas between the PM and the PE.

Table 7. Comparison of steel areas between the PM and the PE. (Source: Own elaboration)

| Model | $A_{smyN}$ (cm²) | $A_{smyP}$ (cm2) | $A_{sminy}$ (cm²) | $A_{spyN}$ (cm²) | $A_{spyP}$ (cm²) | $A_{smxw1}$ (cm²) | $A_{sminxw1}$ (cm²) | $A_{spxw1}$ (cm²) | $A_{smxw2}$ (cm²) | $A_{sminxw2}$ (cm²) | $A_{spxw2}$ (cm²) | $A_{sti}$ (cm²) | $A_{sts}$ (cm²) |
|---|---|---|---|---|---|---|---|---|---|---|---|---|---|
| **PM** | 5.15 | 65.72 | 48.48 | 48.48 | 65.72 | 7.29 | 11.43 | 11.43 | 3.42 | 11.43 | 11.43 | 50.54 | 64.80 |
| **PE** | 3.53 | 58.35 | 84.62 | 84.62 | 84.62 | 19.45 | 20.13 | 20.13 | 16.22 | 20.13 | 20.13 | 67.78 | 91.80 |

where: $A_{smyN}$ and $A_{smyP}$ are the steel areas provided by the negative (bottom) and positive (top) moments in the Y direction, $A_{sminy}$ is the minimum steel area in the Y direction, $A_{spyN}$ and $A_{spyP}$ are the steel areas proposed by the negative (bottom) and positive (top) moments in the Y direction, $A_{smxw1}$ and $A_{smxw2}$ are the steel areas below the column provided by the moments $M_{uf}$ and $M_{ug}$ in the X direction, $A_{sminxw1}$ and $A_{sminxw2}$ are the minimum steel areas below columns 1 and 2 in the X direction, $A_{spxw1}$ and $A_{spxw2}$ are the proposed steel areas below each column in the X direction, $A_{sti}$ is the area per temperature at the bottom of the footing in the X direction with a width $L_y - w_1 - w_2$, $A_{sts}$ is the area per temperature at the top of the footing in the X direction with a width $L_y$.

Table 7 indicates that PM is less than PE for all steel areas.
Therefore, the volumes of concrete and steel for PM are $V_c$ = 9.97 m$^3$ and $V_s$ = 107216.00 cm$^3$, and for PE are $V_c$ = 16.66 m$^3$ and $V_s$ = 167491.20 cm$^3$. Therefore, the savings for concrete is 40.16% of the PM with respect to the PE, and for steel it is 35.99% of the PM with respect to the PE.

## 5. CONCLUSIONS

This paper presents the complete design for determining the thickness and longitudinal and transverse steel areas of RCFs rigid subjected to biaxial and uniaxial flexure on elastic soils (linear soil pressure distribution). The work presented by Montes-Páramo et al. (2023) shows the minimum surface required for RCFs under uniaxial and biaxial flexure.
The main conclusions of this work are:

1. Some authors present the complete design for RCFs subjected to biaxial and uniaxial flexure on elastic soils, but only consider case I (area is fully compressed).
2. This work presents a significant saving in the volumes of concrete and steel compared to the current model for biaxial flexure with a saving for concrete of up to 96.64% and for steel of up to 96.52% with both ends constrained at $L$ = 6.00 m (see figure 11).
3. The proposed model shows savings in the volumes of concrete and steel compared to the current model for uniaxial flexure (case X) with a savings for concrete of up to 84.68% and for steel of up to 85.47% when the load is on the X axis at $L$ = 6.00 m (see figure 12).
4. The current model presents a saving in the volumes of concrete and steel compared to the proposed model for uniaxial flexure (case Y) with a saving for concrete of up to 35.86% and for steel of up to 5.91% when the load is on the Y axis at $L$ = 6.00 m (see figure 12).
5. The thicknesses for biaxial flexure for footings with both ends free and constrained at $L_{y2}$ are governed by $V_{um}$ (Case I) and $V_{uj}$ (Case IV) at $L$ = 6.00 and 7.00 m. For footings with both ends constrained and constrained at $L_{y1}$, they are governed by $M_{ug}$ (Case I) and $V_{uj}$ (Case II) at $L$ = 6.00 m, and by $V_{um}$ (Case I) and $V_{uj}$ (Case II) at $L$ = 7.00 m (see Table 1).
6. The thicknesses for uniaxial flexure for the footings (Case Y) are governed by $V_{uj}$ (Cases Y-1 and Y-II) at $L$ = 6.00 and 7.00 m. The thicknesses for uniaxial flexure for the footings (Case X) are governed by $V_{um}$ (Case X-1) at $L$ = 6.00 and 7.00 m, by $V_{ul}$ and $V_{um}$ (Case X-II) at $L$ = 6.00 and 7.00 m (see Table 2).
7. The comparison between PM and PE proposed by Luévanos-Rojas (2016a) results in a savings for concrete of 40.16% in PM compared to PE, and for steel of 35.99% in PM compared to PE.
8. The PE proposed by Luévanos-Rojas (2016a) was verified through case I of this article and the results coincide.
9. The model proposed in this work can be used for other types of building codes or regulations, simply by considering the resisting moments, flexural shearing strengths, and punching shearing strengths to define the effective depth, and the equations for obtaining the reinforcing steel areas specified by each code or regulation.

10. The proposed model can be used when the resultant force *R* is located outside the central nucleus and within the RCF area, and the current model can be used when the resultant force *R* is located within the central nucleus.

This study presents a robust and effective solution that is applied only to obtain the complete design (thickness and areas of transverse and longitudinal steel), based on the work presented by Montes-Páramo et al. (2023) that determine the sides and minimum area of the RCFs that rest on elastic soils.

Suggestions for future research:

1. Complete design for combined trapezoidal, shaped T-shaped and L-shaped (corner) footings that work partially under compression.
2. Design software for the complete design of RCFs, taking into account the contact area with the soil that works partially under compression.

## 6. REFERENCES

ACI 318S-19 (2019). "*Building Code Requirements for Structural Concrete and Commentary*, Committee 318", New York, USA.

Al-Gahtani, H. J., Adekunle, S. K. (2019), *A boundary-type approach for the computation of vertical stresses in soil due to arbitrarily shaped foundations*. World Journal of Engineering, 16(3), 419-426. https://doi.org/10.1108/WJE-02-2018-0051

Algin, H. M. (2000), *Stresses from linearly distributed pressures over rectangular areas*. International Journal Numerical Analytical Methods in Geomechanics, 24(8), 681-692. https://doi.org/10.1002/1096-9853(200007)24:8<681::AID-NAG89>3.0.CO;2-X

Algin, H. M. (2001), *Vertical stress formula for pressure over rectangular areas*. Géotechnique, 51(8), 719-722. https://doi.org/10.1680/geot.2001.51.8.719

Algin, H. M. (2007), *Practical formula for dimensioning a rectangular footing*. Engineering Structures, 29(6), 1128-1134. https://doi.org/10.1016/j.engstruct.2006.08.009

Aydogdu, I. (2016), *New Iterative method to Calculate Base Stress of Footings under Biaxial Bending*. International Journal of Engineering & Applied Sciences (IJEAS), 8(4), 40-48. https://doi.org/10.24107/ijeas.281460

Bezmalinovic Colleoni, A. S. (2016), *Fórmulas Analíticas para la Presión de Contacto Lineal en Fundaciones Rectangulares Altamente Excéntricas*. IX Chilean Congress on Geotechnical Engineering, Chilean Geotechnical Society, Universidad Austral de Chile.

Dagdeviren, U. (2016), *Shear stresses below the rectangular foundations subjected to biaxial bending*. Geomechanics Engineering, 10(2), 189-205. https://doi.org/10.12989/gae.2016.10.2.189

Galvis, F. A., Smith-Pardo, P. J. (2020), *Axial load biaxial moment interaction (PMM) diagrams for shallow foundations: Design aids, experimental verification, and examples*. Engineering Structures, 213, 110582. https://doi.org/10.1016/j.engstruct.2020.110582

Girgin, K. (2017), *Simplified formulations for the determination of rotational spring constants in rigid spread footings resting on tensionless soil*. Journal of Civil Engineering and Management, 23(4), 464-474. https://doi.org/10.3846/13923730.2016.1210218

Gör, M. (2022), *Analyzing the bearing capacity of shallow foundations on two-layered soil using two novel cosmology-based optimization techniques*. Smart Structures and Systems, 29(3), 513-522. https://doi.org/10.12989/sss.2022.29.3.513

Highter, W. H., Anders, J. C. (1985), *Dimensioning Footings Subjected to Eccentric Loads*. Journal of Geotechnical Engineering ASCE, 111(5), 659-665. https://doi.org/10.1061/(ASCE)0733-9410(1985)111:5(659)

Irles-Más, R., Irles-Más, F. (1992), *Alternativa analítica a la determinación de tensiones bajo zapatas rectangulares con flexión biaxial y despegue parcial*. Informes de la Construcción, 44(419), 77-89. https://dialnet.unirioja.es/servlet/articulo?codigo=2768804
Kaur, A., Kumar, A. (2016), *Behavior of eccentrically inclined loaded footing resting on fiber reinforced soil*. Geomechanics Engineering, 10(2), 155-174. https://doi.org/10.12989/gae.2016.10.2.155
Kim-Sánchez, D. S., Luévanos-Rojas, A., Barquero-Cabrero, J. D., López-Chavarría, S., Medina-Elizondo, M., Luévanos-Soto, I. (2022), *A new model for the complete design of circular isolated footings considering that the contact surface works partially under compression*. International Journal of Innovative Computing, Information and Control, 18(6), 1769-1784. http://www.ijicic.org/ijicic-180607.pdf
Konapure, C. G., Vivek, B. (2013), *Analysis of Combined rectangular footing by Winkler's Model and Finite Element Method*. International Journal of Engineering and Innovative Technology, 3(5), 128-132. https://www.ijeit.com/Vol%203/Issue%205/IJEIT1412201311_21.pdf
Lee, J., Jeong, S., Lee, J. K. (2015), *3D analytical method for mat foundations considering coupled soil springs*. Geomechanics Engineering, 8(6), 845-850. https://doi.org/10.12989/gae.2015.8.6.845
Lezgy-Nazargah, M., Mamazizi, A., Khosravi, H. (2022), *Analysis of shallow footings rested on tensionless foundations using a mixed finite element model*. Structural Engineering and Mechanics, 81(3), 379-394. https://doi.org/10.12989/sem.2022.81.3.379
Luévanos-Rojas, A. (2014), *Design of boundary combined footings of rectangular shape using a new model*. DYNA, 81(188), 199-208. https://doi.org/10.15446/dyna.v81n188.41800
Luévanos-Rojas, A. (2016a), *Un nuevo modelo para diseño de zapatas combinadas rectangulares de lindero con dos lados opuestos restringidos*. Revista ACONPAT, 6(2), 173-189. http://dx.doi.org/10.21041/ra.v6i2.137
Luévanos-Rojas, A. (2016b), *A Mathematical Model for the Dimensioning of Combined Footings of Rectangular Shape*. Revista Técnica de la Facultad de Ingeniería Universidad del Zulia, 39(1), 3-9. http://ve.scielo.org/scielo.php?script=sci_abstract&pid=S0254-07702016000100002&lng=en&nrm=iso&tlng=es
Luévanos-Rojas, A. (2023), *Nuevo modelo para el diseño completo de zapatas aisladas rectangulares tomando en cuenta que la superficie de contacto funciona parcialmente en compresión*. Revista ALCONPAT, 13(2), 192-219. https://doi.org/10.21041/ra.v13i2.671
Luévanos-Rojas, A., Barquero-Cabrero, J. D., López-Chavarría, S., Medina-Elizondo, M. (2017), *A comparative study for design of boundary combined footings of trapezoidal and rectangular forms using new models*. Coupled Systems Mechanics, 6(4), 417-437. https://doi.org/10.12989/csm.2017.6.4.417
Luévanos-Rojas, A., López-Chavarría, S., Medina-Elizondo, M., Sandoval-Rivas, R., Farías-Montemayor, O. M. (2020), *Un modelo analítico para el diseño de zapatas combinadas de esquina*. Revista ALCONPAT, 10 (3), 317-335. https://doi.org/10.21041/ra.v10i3.432
Luévanos-Rojas, A. (2025a), *Optimal surface for corner combined footings assuming that the ground contact area works partially in compression considering that the maximum pressure is located at the corner of the footing: Part 1*. Advances in Concrete Construction, 19(6), 349-362. https://doi.org/10.12989/acc.2025.19.6.349
Luévanos-Rojas, A. (2025b), *Optimal surface for corner combined footings assuming that the ground contact area works partially in compression considering that the maximum pressure is located at one end and on the outer and inner side of the footing: Part 2*. Advances in Concrete Construction, 19(6), 363-380. https://doi.org/10.12989/acc.2025.19.6.363
Luévanos-Rojas, A., Estrada-Mendoza, B. L., Juárez-Ramírez, M., (2025), *Área óptima para zapatas combinadas en forma de T asumiendo que el área en contacto con el suelo trabaja*

*parcialmente en compresión*. Boletín de Ciencias de la Tierra, 58(2), 51-71. https://doi.org/10.15446/rbct.n58.120221

Luévanos-Soto, I., Luévanos-Rojas, A., Moreno-Landeros, V. M., Santiago-Hurtado, G., (2024a), *Minimum area for circular isolated footings with eccentric column taking into account that the surface in contact with the ground works partially in compression*. Coupled Systems Mechanics, 13(3), 201-217. https://doi.org/10.12989/csm.2024.13.3.201

Luévanos-Soto, I., Luévanos-Rojas, A., Moreno-Landeros, V. M., Santiago-Hurtado, G., (2024b), *Minimum cost design for circular isolated footings with eccentric column taking into account that the surface in contact with the ground works partially in compression*. Coupled Systems Mechanics, 13(4), 311-335. https://doi.org/10.12989/csm.2024.13.4.311

Montes-Paramo, P., Luévanos-Rojas, A., López-Chavarría, S., Medina-Elizondo, M., Sandoval-Rivas, R. (2023), *Área óptima para zapatas combinadas rectangulares asumiendo que la superficie de contacto con el suelo trabaja parcialmente a compresión*. Ingeniería Investigación y Tecnología, 24(02), 1-15. https://doi.org/10.22201/fi.25940732e.2023.24.2.012

Özmen, G. (2011), *Determination of Base Stresses in Rectangular Footings under Biaxial Bending*. Teknik Dergi Digest, 22(4), 1519-1535. http://www.imo.org.tr/resimler/dosya_ekler/7b559795bd3f63b_ek.pdf?dergi=472

Peck, R. B., Hanson, W. E., Thornburn, T. H. (1974), "*Foundation Engineering*", 2nd ed. New York: John Wiley and Sons.

Ravi Kumar Reddy, C., Satish Kumar, M., Kondala Rao, M., Gopika, N. (2018), *Numerical Analysis of Rectangular Combined Footings Resting on Soil for Contact Pressure*. International Journal of Civil Engineering and Technology, 9(9), 1425-1431. http://iaeme.com/Home/issue/IJCIET?Volume=9&Issue=9

Rawat, S., Mittal, R. K., Muthukumar, G. (2020), *Isolated Rectangular Footings under Biaxial Bending: A Critical Appraisal and Simplified Analysis Methodology*. Practice Periodical on Structural Design and Construction, 25(3). https://doi.org/10.1061/(ASCE)SC.1943-5576.0000471

Rodriguez-Gutierrez, J. A., Aristizabal-Ochoa, J. D. (2004), *Presiones en zapatas rígidas de forma arbitraria sometidas a carga axial excéntrica*. Revista Internacional de Desastres Naturales, Accidentes e Infraestructura Civil, 4(1), 67-82. https://www.scipedia.com/wd/images/2/27/Draft_Content_636675925Rodriguez-Gutierrez_Aristizabal-Ochoa_a.pdf

Rodriguez-Gutierrez, J. A., Aristizabal-Ochoa, J. D. (2013a), *Rigid Spread Footings Resting on Soil Subjected to Axial Load and Biaxial Bending. I: Simplified Analytical Method*. Internacional Journal of Geomechanics-ASCE, 13(2), 109-119. https://doi.org/10.1061/(ASCE)GM.1943-5622.0000218

Rodriguez-Gutierrez, J. A., Aristizabal-Ochoa, J. D. (2013b), *Rigid Spread Footings Resting on Soil Subjected to Axial Load and Biaxial Bending. II: Design Aids*. Internacional Journal of Geomechanics-ASCE, 13(2), 120-131. https://doi.org/10.1061/(ASCE)GM.1943-5622.0000210

Soto-Garcia, S., Luévanos-Rojas, A., Barquero-Cabrero, J. D., López-Chavarría, S., Medina-Elizondo, M., Farias-Montemayor, O. M., Martinez-Aguilar, C. (2022), *A New Model for the Contact Surface With Soil of Circular Isolated Footings Considering that the Contact Surface Works Partially Under Compression*. International Journal of Innovative Computing, Information and Control, 18(4), 1103-1116. http://www.ijicic.org/ijicic-180406.pdf

Teng, W. C. (1979), "*Foundation Design*", New Jersey: Prentice-Hall Inc.

Vela-Moreno, V. B., Luévanos-Rojas, A., López-Chavarría, S., Medina-Elizondo, M., Sandoval-Rivas, R., Martinez-Aguilar, C. (2022), *Optimal area for rectangular isolated footings considering that contact surface works partially to compression*. *Structural Engineering and Mechanics*, 84(4), 561-573. https://doi.org/10.12989/sem.2022.84.4.561

Velazquez-Santillan, F., Luévanos-Rojas, A., Lopez-Chavarria, S., Medina-Elizondo, M., Sandoval-Rivas, R. (2018), *Numerical experimentation for the optimal design for reinforced concrete rectangular combined footings*. Advances in Computational Design, 3(1), 49-69. https://doi.org/10.12989/acd.2018.3.1.049

Vitone, D. M. A., Valsangkar, A. J. (1986), *Stresses from Loads over Rectangular Areas*. Journal of Geotechnical Engineering ASCE, 112(10), 961-964. https://doi.org/10.1061/(ASCE)0733-9410(1986)112:10(961)

Vivek, B., Arkal, L. S., Bandgar, R. V., Kalekhan, F. A. S. (2014), *Comparative Study on Conventional and Simplified Elastic Analysis of Rectangular Combined Footing*. International Journal of Research in Engineering and Technology, 3(4), 422-427. https://ijret.org/volumes/2014v03/i04/IJRET20140304076.pdf

Young, W. C., Budynas, R. G. (2002), *Roark's Formulas for Stress and Strain*. 7th ed. New Jersey: McGraw-Hill.

## ANNEX

Table 1. Examples of biaxial flexure.
(Source: Own elaboration)

| Concept | Free ends; constrained in $L_{y2}$ | | | | Constrained ends; constrained in $L_{y1}$ | | | |
|---|---|---|---|---|---|---|---|---|
| Case | I | IV | 1 | IV | I | II | I | II |
| $L$ (m) | 6.00 | | 7.00 | | 6.00 | | 7.00 | |
| $R_u$ (kN) | 2040 | 2040 | 2040 | 2040 | 2040 | 2040 | 2040 | 2040 |
| $M_{uxT}$ (kN-m) | 0 | 0 | 0 | 0 | 2040 | 2040 | 1700 | 1700 |
| $M_{uyT}$ (kN-m) | 1020 | 1020 | 1020 | 1020 | 1020 | 1020 | 1020 | 1020 |
| $L_x$ (m) | 3.00 | 2.19 | 3.00 | 2.10 | 48.00 | 3.48 | 9.25 | 2.89 |
| $L_y$ (m) | 8.40 | 8.40 | 9.07 | 9.07 | 6.40 | 6.40 | 7.40 | 7.40 |
| $L_{y1}$ (m) | 2.20 | 2.20 | 1.87 | 1.87 | 0.20 | 0.20 | 0.20 | 0.20 |
| $L_{y2}$ (m) | 0.20 | 0.20 | 0.20 | 0.20 | 0.20 | 0.20 | 0.20 | 0.20 |
| $L_{x3}$ (m) | - | 1.79 | - | 1.65 | - | 5.32 | - | 3.64 |
| $L_{y3}$ (m) | - | 444529.09 | - | 434025.46 | - | 9.06 | - | 13.94 |
| $d_p$ (cm) | 82 | 77 | 82 | 82 | 132 | 57 | 102 | 67 |
| $r$ (cm) | 8 | 8 | 8 | 8 | 8 | 8 | 8 | 8 |
| $t$ (cm) | 90 | 85 | 90 | 90 | 140 | 65 | 110 | 75 |
| $V_c$ (m$^3$) | 22.45 | 15.46 | 24.25 | 16.95 | 424.75 | 14.29 | 74.52 | 15.72 |
| $M_{ua}$ (kN-m) | -485.71 | -486.88 | -312.50 | -312.91 | 0 | 0 | 0 | 0 |
| $M_{ub}$ (kN-m) | 796.57 | 794.90 | 1015.50 | 1015.24 | 1447.59 | 1446.16 | 1459.58 | 1458.68 |
| $y_c$ (m) | 1.40 | 1.40 | 1.51 | 1.50 | 1.99 | 1.98 | 2.09 | 2.11 |
| $M_{uc}$ (kN-m) | 816.00 | 816.01 | 1118.22 | 1118.71 | 1622.28 | 1601.34 | 1755.12 | 1743.22 |
| $M_{ud}$ (kN-m) | -2467.43 | -2485.99 | -2466.00 | -2449.84 | -2450.59 | -2449.90 | -2455.69 | -2467.56 |
| $M_{ue}$ (kN-m) | 0 | 0 | 0 | 0 | 0 | 0 | 0 | 0 |
| $Ø_fM_{ux}$ (kN-m) | 7608.05 | 3480.81 | 9868.15 | 6907.71 | 409143.86 | 5531.16 | 47079.19 | 6346.50 |
| $M_{uf}$ (kN-m) | -327.73 | -127.46 | -327.73 | -119.88 | -4180.16 | -216.06 | -878.70 | -152.72 |
| $Ø_fM_{uf}$ (kN-m) | 4013.05 | 3393.55 | 4013.05 | 4013.05 | 9035.26 | 1088.75 | 4631.57 | 1614.08 |
| $M_{ug}$ (kN-m) | -655.47 | -85.52 | -655.47 | -79.59 | -8360.32 | -362.38 | -1757.40 | -230.52 |
| $Ø_fM_{ug}$ (kN-m) | 2664.40 | 2276.87 | 2664.40 | 2664.40 | 9035.26 | 1088.75 | 4631.57 | 1614.08 |
| $V_{uh}$ (kN) | -485.71 | -486.88 | -190.50 | -374.75 | * | * | * | * |
| $V_{ui}$ (kN) | -102.00 | -91.70 | 30.50 | 31.49 | -244.10 | 50.64 | 74.80 | 189.92 |
| $V_{uj}$ (kN) | -1063.71 | -1080.04 | -1085.50 | -1081.51 | -1187.60 | -1274.09 | -1182.28 | -1225.93 |
| $V_{uk}$ (kN) | * | * | * | * | * | * | * | * |
| $Ø_vV_{ux}$ (kN) | 1628.97 | 1116.64 | 1628.97 | 1140.28 | 41955.86 | 1313.50 | 6247.69 | 1282.18 |
| $V_{ul}$ (kN) | -200.19 | -39.78 | -219.04 | -9.96 | -329.05 | -176.74 | -301.61 | -113.30 |
| $Ø_vV_{ul}$ (kN) | 662.45 | 258.55 | 662.45 | 662.45 | 926.53 | 258.55 | 614.64 | 326.09 |
| $V_{um}$ (kN) | -400.38 | -26.69 | -400.38 | -6.61 | -658.10 | -57.05 | -603.22 | -55.58 |
| $Ø_vV_{um}$ (kN) | 439.82 | 400.26 | 439.82 | 439.82 | 926.53 | 258.55 | 614.64 | 326.09 |
| $V_{up1}$ (kN) | 599.59 | 535.43 | 605.50 | 532.79 | 658.42 | 565.21 | 618.67 | 556.64 |
| $Ø_vV_{up1}$ (kN) | 5143.71 | 4632.11 | 5143.71 | 5143.71 | 6515.50 | 1714.48 | 4248.03 | 2187.51 |
| $V_{up2}$ (kN) | 1280.00 | 1263.01 | 1285.91 | 1262.26 | 1357.36 | 1359.22 | 1344.31 | 1338.92 |
| $Ø_vV_{up2}$ (kN) | 2993.47 | 2711.96 | 2993.47 | 2993.47 | 6515.50 | 1714.48 | 4248.03 | 2187.51 |
| $A_{smyN}$ (cm$^2$) | 82.89 | 91.22 | 82.84 | 83.84 | 49.16 | 122.62 | 64.21 | 104.00 |
| $A_{smyP}$ (cm$^2$) | 26.67 | 28.61 | 36.72 | 37.03 | 32.53 | 77.92 | 45.78 | 71.98 |
| $A_{sminy}$ (cm$^2$) | 81.92 | 56.15 | 81.92 | 57.34 | 2109.89 | 66.05 | 314.19 | 64.48 |
| $A_{spyN}$ (cm$^2$) | 82.89 | 91.22 | 82.84 | 83.84 | 2109.89 | 122.62 | 314.19 | 104.00 |
| $A_{spyP}$ (cm$^2$) | 81.92 | 56.15 | 81.92 | 57.34 | 2109.89 | 77.92 | 314.19 | 71.98 |
| $A_{smxw1}$ (cm$^2$) | 10.71 | 4.40 | 10.71 | 3.89 | 90.69 | 10.35 | 23.49 | 6.12 |
| $A_{sminxw1}$ (cm$^2$) | 33.31 | 30.00 | 33.31 | 33.31 | 46.59 | 13.00 | 30.91 | 16.40 |
| $A_{spxw1}$ (cm$^2$) | 33.31 | 30.00 | 33.31 | 33.31 | 90.69 | 13.00 | 30.91 | 16.40 |
| $A_{smxw2}$ (cm$^2$) | 22.00 | 2.96 | 22.00 | 2.58 | 201.79 | 17.77 | 48.59 | 9.31 |
| $A_{sminxw2}$ (cm$^2$) | 22.12 | 20.13 | 22.12 | 22.12 | 46.59 | 13.00 | 30.91 | 16.40 |
| $A_{spxw2}$ (cm$^2$) | 22.12 | 20.13 | 22.12 | 22.12 | 201.79 | 17.77 | 48.59 | 16.40 |
| $A_{sti}$ (cm$^2$) | 103.19 | 98.61 | 114.05 | 114.05 | 94.75 | 58.85 | 110.48 | 80.06 |
| $A_{sts}$ (cm$^2$) | 136.08 | 128.52 | 146.93 | 146.93 | 161.28 | 74.88 | 146.52 | 99.90 |
| $V_s$ (cm$^3$) | 226850.40 | 184510.74 | 244360.32 | 194496.36 | 5333507.20 | 185591.60 | 776263.70 | 321938.04 |

* It does not exist because the axis is located outside the footing area.

Table 2. Examples of uniaxial flexure.
(Source: Own elaboration)

| Concept | Loads located on the Y axis | | | | Loads located on the X axis | | | |
|---|---|---|---|---|---|---|---|---|
| **Case** | **Y-I** | **Y-II** | **Y-I** | **Y-II** | **X-I** | **X-II** | **X-I** | **X-II** |
| $L$ (m) | 6.00 | | 7.00 | | 6.00 | | 7.00 | |
| $R_u$ (kN) | 1360 | 1360 | 1360 | 1360 | 1360 | 1360 | 1360 | 1360 |
| $M_{uxT}$ (kN-m) | 1954.43 | 2210.22 | 2278.00 | 2291.60 | 0 | 0 | 0 | 0 |
| $M_{uyT}$ (kN-m) | 0 | 0 | 0 | 0 | 4080 | 4080 | 4080 | 4080 |
| $L_x$ (m) | 1.00 | 1.03 | 1.00 | 1.00 | 18.00 | 7.04 | 18.00 | 6.90 |
| $L_y$ (m) | 9.53 | 9.75 | 10.05 | 10.03 | 6.40 | 6.40 | 7.40 | 7.40 |
| $L_{y1}$ (m) | 3.33 | 3.25 | 2.85 | 2.83 | 0.20 | 0.20 | 0.20 | 0.20 |
| $L_{y2}$ (m) | 0.20 | 0.50 | 0.20 | 0.20 | 0.20 | 0.20 | 0.20 | 0.20 |
| $L_{x3}$ (m) | - | - | - | - | - | 1.56 | - | 1.35 |
| $L_{y3}$ (m) | - | 9.75 | - | 10.00 | - | - | - | - |
| $d_p$ (cm) | 97 | 97 | 102 | 102 | 107 | 37 | 92 | 37 |
| $r$ (cm) | 8 | 8 | 8 | 8 | 8 | 8 | 8 | 8 |
| $t$ (cm) | 105 | 105 | 110 | 110 | 115 | 45 | 100 | 45 |
| $V_c$ (m$^3$) | 9.87 | 15.39 | 10.91 | 10.88 | 131.02 | 20.07 | 131.67 | 22.74 |
| $M_{ua}$ (kN-m) | -1190.72 | -1162.41 | -866.78 | -858.23 | 0 | 0 | 0 | 0 |
| $M_{ub}$ (kN-m) | 3.52 | 31.45 | 364.50 | 373.51 | 119.00 | 119.00 | 121.30 | 121.30 |
| $y_c$ (m) | 1.84 | 2.02 | 2.08 | 2.09 | 0 | 0 | 0 | 0 |
| $M_{uc}$ (kN-m) | 37.03 | 65.28 | 365.58 | 374.48 | 952.00 | 952.00 | 1122.00 | 1122.00 |
| $M_{ud}$ (kN-m) | -2585.37 | -2585.64 | -2584.29 | -2579.70 | 119.00 | 119.00 | 121.30 | 121.30 |
| $M_{ue}$ (kN-m) | 0 | -0.13 | 0 | 0 | 0 | 0 | 0 | 0 |
| $Ø_f M_{ux}$ (kN-m) | 4602.89 | 4740.97 | 5089.64 | 5089.64 | 100815.43 | 4714.80 | 74530.68 | 4621.04 |
| $M_{uf}$ (kN-m) | -30.60 | -9.24 | -30.60 | -8.66 | -2120.09 | -347.52 | -2120.09 | -300.74 |
| $Ø_f M_{uf}$ (kN-m) | 6305.96 | 6305.96 | 7227.29 | 7227.29 | 5236.80 | 391.78 | 3560.91 | 391.78 |
| $M_{ug}$ (kN-m) | -30.60 | -8.00 | -30.60 | -5.55 | -2777.43 | -347.52 | -2777.43 | -300.74 |
| $Ø_f M_{ug}$ (kN-m) | 4073.56 | 5454.42 | 4631.57 | 4631.57 | 5236.80 | 391.78 | 3560.91 | 391.78 |
| $V_{uh}$ (kN) | -523.93 | -520.57 | -405.38 | -402.67 | * | * | * | * |
| $V_{ui}$ (kN) | -268.85 | -277.62 | -198.49 | -198.53 | 367.63 | 516.38 | 437.41 | 538.49 |
| $V_{uj}$ (kN) | -635.95 | -645.71 | -652.85 | -653.72 | -367.63 | -516.38 | -437.41 | -538.49 |
| $V_{uk}$ (kN) | * | * | * | * | * | * | * | * |
| $Ø_v V_{ux}$ (kN) | 642.32 | 661.59 | 675.43 | 675.43 | 12753.63 | 1724.85 | 10965.74 | 1690.55 |
| $V_{ul}$ (kN) | * | * | * | * | -403.10 | -124.11 | -409.27 | -107.41 |
| $Ø_v V_{ul}$ (kN) | 879.97 | 879.97 | 959.10 | 959.10 | 662.48 | 143.33 | 523.92 | 143.33 |
| $V_{um}$ (kN) | * | * | * | * | -625.25 | -124.11 | -520.85 | -107.41 |
| $Ø_v V_{um}$ (kN) | 568.45 | 761.15 | 614.64 | 614.64 | 662.48 | 143.33 | 523.92 | 143.33 |
| $V_{up1}$ (kN) | 431.22 | 424.12 | 404.17 | 394.76 | 663.77 | 680.00 | 668.41 | 680.00 |
| $Ø_v V_{up1}$ (kN) | 6832.74 | 6832.74 | 7447.17 | 7447.17 | 4593.81 | 922.67 | 3595.04 | 922.67 |
| $V_{up2}$ (kN) | 657.36 | 659.83 | 669.52 | 669.48 | 663.77 | 680.00 | 668.41 | 680.00 |
| $Ø_v V_{up2}$ (kN) | 3915.11 | 3915.11 | 4248.03 | 4248.03 | 4593.81 | 922.67 | 3595.04 | 922.67 |
| $A_{smyN}$ (cm$^2$) | 77.86 | 77.61 | 73.21 | 73.07 | 0 | 0 | 0 | 0 |
| $A_{smyP}$ (cm$^2$) | 1.01 | 1.78 | 9.59 | 9.82 | 23.57 | 70.30 | 32.34 | 83.43 |
| $A_{sminy}$ (cm$^2$) | 32.30 | 33.27 | 33.97 | 33.97 | 641.36 | 86.74 | 551.45 | 85.01 |
| $A_{spyN}$ (cm$^2$) | 77.86 | 77.61 | 73.21 | 73.07 | 641.36 | 86.74 | 551.45 | 85.01 |
| $A_{spyP}$ (cm$^2$) | 32.30 | 33.27 | 33.97 | 33.97 | 641.36 | 86.74 | 551.45 | 85.01 |
| $A_{smxw1}$ (cm$^2$) | 0.84 | 0.25 | 0.79 | 0.22 | 56.12 | 25.19 | 67.80 | 24.86 |
| $A_{sminxw1}$ (cm$^2$) | 44.25 | 44.25 | 48.23 | 48.23 | 33.31 | 7.21 | 26.35 | 7.21 |
| $A_{spxw1}$ (cm$^2$) | 44.25 | 44.25 | 48.23 | 48.23 | 56.12 | 25.19 | 67.80 | 24.86 |
| $A_{smxw2}$ (cm$^2$) | 0.84 | 0.22 | 0.79 | 0.14 | 75.35 | 25.19 | 92.62 | 24.86 |
| $A_{sminxw2}$ (cm$^2$) | 28.59 | 38.28 | 30.91 | 30.91 | 33.31 | 7.21 | 26.35 | 7.21 |
| $A_{spxw2}$ (cm$^2$) | 28.59 | 38.28 | 30.91 | 30.91 | 75.35 | 25.19 | 92.62 | 24.86 |
| $A_{sti}$ (cm$^2$) | 104.76 | 135.99 | 152.86 | 152.46 | 93.77 | 42.36 | 102.24 | 50.46 |
| $A_{sts}$ (cm$^2$) | 180.12 | 184.28 | 198.99 | 198.59 | 132.48 | 51.84 | 133.20 | 59.94 |
| $V_s$ (cm$^3$) | 140754.48 | 149596.40 | 150814.90 | 150380.12 | 1464836.80 | 212811.52 | 1528694.00 | 236297.60 |